Article:

Cosgrove, GIE, Colombera, L and Mountney, NP (2021) A database of Aeolian Sedimentary Architecture for the characterization of modern and ancient sedimentary systems. Marine and Petroleum Geology, 127. 104983. ISSN: 0264-8172

https://doi.org/10.1016/j.marpetgeo.2021.104983

TITLE: A Database of Aeolian Sedimentary Architecture for the characterization of modern and ancient sedimentary systems

AUTHORS: Cosgrove, G.I.E[1]*., Colombera, L. [1], Mountney, N.P. [1]

***Corresponding Author:** g.i.e.cosgrove@leeds.ac.uk

[1] Fluvial, Eolian & Shallow-Marine Research Group, School of Earth and Environment, The University of Leeds, LS2 9JT, UK

Highlights

- The Database of Aeolian Sedimentary Architecture (DASA) is a novel relational database designed to record attributes of modern and ancient aeolian systems
- DASA stores data on a variety of aeolian and associated non-aeolian entities at multiple scales
- DASA allows quantitative characterization and comparisons of modern and ancient aeolian sedimentary systems
- DASA is a valuable tool for constraining lithological heterogeneity in subsurface aeolian successions

Abstract

The Database of Aeolian Sedimentary Architecture (DASA) records the architecture and spatio-temporal evolution of a broad range of modern and recently active aeolian systems, and of their preserved deposits in ancient successions. DASA currently stores data on >14,000 geologic and geomorphic entities (including bounding surfaces and transition relationships) extracted from >60 case-study examples documented in the published literature. DASA stores data on a variety of aeolian and associated non-aeolian entities of multiple scales, including attributes that characterize their type, geometry, spatial relations, hierarchical relations, temporal significance, and textural and petrophysical properties; associated metadata are also stored.

Database output describes (1) stratigraphic relationships between aeolian and associated fluvial, lacustrine and paralic depositional systems; (2) the geometry of aeolian architectural elements, and hierarchical and spatial relationships between them; (3) the probabilities of vertical and lateral transition from one type of deposit or landform to another; (4) the presence and nature of aeolian bounding surfaces at different scales, and their nested, hierarchical relationships; (5) aeolian lithofacies types, proportions and distributions, and (6) grain-scale textural parameters.

DASA is applied to quantitatively characterize and compare modern and ancient aeolian sedimentary systems. Examples of database outputs demonstrate how DASA outputs can be tailored for numerous applications, including: (1) the development of bespoke quantitative facies models, specifically tailored for particular sets of boundary conditions; (2) the empirical assessment of how aeolian systems, and associated preserved sedimentary architectures, represent a response to allogenic and autogenic forcings; and (3) the instruction of forward stratigraphic models and 3D geocellular subsurface models. DASA is a valuable tool for the characterization of subsurface aeolian successions, such that output can help to (1) predict three-dimensional lithological heterogeneity in subsurface successions that are resource targets, (2) constrain geocellular stochastic models, and (3) facilitate borehole correlations of aeolian dune sets or associated non-aeolian elements.

Keywords

Database, sedimentary architecture, reservoir, quantitative geology, aeolian, metadata, geomorphic, dune

1. Introduction

The preserved aeolian sedimentary record spans over three billion years of Earth history from the Archean to present day (e.g., Clemmensen, 1985; Dott et al., 1986; Voss, 2002; Cather et al., 2008; Simpson et al., 2012; Rodríguez-López et al., 2014). Despite an extensive global sedimentary record (e.g., Ridgley, 1977; Ross, 1981; Bateman et al., 2004; Holz et al., 2008; Dong et al., 2010) and recent extra-planetary observations (e.g., Grotzinger et al., 2005; Metz et al., 2009; Banham et al., 2018), meaningful comparisons between aeolian systems developed under differing controlling factors are not straightforward. Traditional aeolian facies models, developed from studies of both modern systems and ancient successions, have attempted to capture stratigraphic complexities (e.g., McKee, 1966; Thompson, 1970a, 1970b; Brookfield, 1977, Kocurek, 1981; Loope, 1984; Langford and Chan, 1988; Mountney and Thompson, 2002; Mountney and Jagger, 2004; Mountney, 2006a; Kocurek and Day, 2018); yet, many such models are largely qualitative or – at best – semi-quantitative, and are commonly case-specific. Thus, individual case studies cannot adequately account for the wide variety of aeolian-system architectures that might potentially develop through the action of a varied range of allogenic and autogenic controls, which govern the geometry and arrangement of architectural elements and their bounding surfaces. However, generalized models have been proposed to explain the primary allogenic and autogenic controls that drive aeolian-system construction, accumulation and preservation in the stratigraphic record (e.g., Kocurek and Havholm, 1993; Kocurek, 1999; Kocurek and Lancaster, 1999). Several such models are quantitative in form (e.g. Rubin, 1987; Rubin and Carter, 2006; Mountney, 2012). Moreover, some studies have generated large quantitative datasets in the form of 3D virtual geological models assembled from mosaics of LiDAR and photogrammetry datasets and presented as geo-models (e.g., Pierce et al., 2016). Numerous studies of modern systems have considerably improved our understanding of the physical conditions that dictate aeolian bedform arrangements (e.g., Bristow et al., 2000a, Kocurek and Ewing, 2005; Beveridge et al., 2006; Kocurek et al., 2007; Derickson et al., 2008; Ewing and Kocurek, 2010).

Despite the above-mentioned advances, it remains difficult to make direct quantitative comparisons between documented examples of individual case studies that describe aeolian systems and their preserved sedimentary architectures (Rodríguez-López et al., 2014). To facilitate the quantitative sedimentological and stratigraphical characterization of aeolian systems, and to enable meaningful comparisons between systems, this study introduces and employs a novel relational database: the Database of Aeolian Sedimentary Architecture (DASA). The use of databasing methodologies in the broader field of sedimentology has increased in recent years (e.g., Baas et al., 2005; Gibling, 2006; Colombera et al., 2012a, 2013, 2016; Cullis et al., 2019). DASA represents the first example of a quantitative, relational database with global coverage, designed specifically to investigate sedimentary relationships within and between modern and ancient aeolian sedimentary successions (Fig. 1). Quantitative data included in DASA are supported by associated qualitative data, including metadata describing age, location and broader environmental setting, together with information relating to original descriptions, interpretations and classifications of forms and deposits.

The aim of this study is to demonstrate the efficacy of using a database-informed approach to advance the quantitative characterization of aeolian systems for the purpose of gaining an improved understanding of the controls that govern patterns of aeolian sedimentation in a wide variety of settings, and over both time and space.

Objectives of this paper are: (1) to present a detailed explanation of the structure of DASA, including explanation of the entities and relationships defined therein; (2) to show multiple examples of how DASA can be queried to produce quantitative data relating to aspects of the sedimentology and sedimentary architecture of modern and ancient aeolian systems; (3) to show examples illustrating how DASA can be sequentially filtered by the user, to provide quantitative architectural metrics for a specific subset of aeolian systems governed by a particular set of controlling conditions; and (4) to show how DASA can facilitate the generation of quantitative geological analogues to subsurface aeolian reservoir successions.

2. Methodology

The Database of Aeolian Sedimentary Architecture is a relational database (see Codd, 1970), in which data are organized into a series of tables (Fig. 2). Each table holds data on one entity type; the rows within each table represent instances (or records) of that entity type and the columns represent attributes (or fields) associated with each entry. In DASA, every table has a column storing a unique numerical identifier (primary key), assigned to each row; rows in one entity table are linked to rows in different entity tables through columns storing the unique numerical identifier of the linked row (foreign key; Fig. 2). This means that the tables (entities) are related by logical connections between them, as established by primary and foreign keys (Figs. 2, 3). The entity-relationship model of DASA is based in part on those of other sedimentological relational databases: the Shallow-Marine Architecture Knowledge Store (SMAKS; Colombera et al., 2016), the Deep-Marine Architecture Knowledge Store (DMAKS; Cullis et al., 2019) and the Fluvial Architecture Knowledge Transfer System (FAKTS; Colombera et al., 2012a).

DASA stores data encompassing aeolian stratigraphy and sedimentology, relating to both modern and ancient systems. A process of data standardization is applied upon data entry to DASA to ensure the use of consistent terminology and to reconcile the variety of source data types (e.g., outcrop, core, well-log, seismic, satellite imagery) that were originally employed to characterize the aeolian systems.

DASA is written in SQL (Structured Query Language) and is managed via the *MariaDB* (*MySQL*) database management system; *HeidiSQL* is used as a database front-end. Information is retrieved from DASA using SQL queries, which return quantitative outputs that can be filtered based on the parameters used to classify aeolian systems. For example, to generate results relating specifically to wet (i.e. water-table influenced) aeolian systems (*sensu* Kocurek and Havholm, 1993), or to wetting- or drying-upwards aeolian systems (e.g., George and Berry, 1993; Howell and Mountney, 1996), or to aeolian systems with a secondary fluvial influence (e.g., Scherer et al., 2007; Formolo Ferronatto et al., 2019; Reis et al., 2020). Additionally, the metadata and ancillary data accompanying each DASA entry can also be used to filter results. For example, to return results relating only to Permian aeolian systems, or only to aeolian systems accumulated in intra-cratonic rift settings, or only to aeolian systems that developed in Pangaean supercontinental settings. The results of queries can be exported in a tabulated form for later processing, using statistical software (e.g., SPSS, Minitab), or accessed directly using a specialized programming language, such as Python or R.

3. Database Structure and Overview

Datasets entered into DASA are organized into case studies; a case study describes a particular modern desert system (e.g., the Idhan Murzuq Desert; Table 1), or ancient aeolian succession (e.g., Entrada Sandstone; Table 2). Case studies are associated with one or more sets of data that are hereafter referred to as 'subsets' (cf. Colombera et al., 2012a). Each subset represents a collection of data (e.g., a sedimentary log or architectural panel) from an original data source (e.g., a publication or thesis). The different subsets of a case study vary in the way they are classified with respect to geological attributes and/or metadata; they are established to facilitate database interrogation (Fig. 3A; Fig. 4A).

Each subset is divided into depositional complexes (Fig. 3B; Fig. 4B-C), which describe both ancient and modern environments. In ancient environments, a depositional complex is defined as a sedimentary body, typically composed of a suite of smaller elements that characterize a net depositional setting. In modern environments, a depositional complex is typically a planform area characterizing a particular depositional setting (e.g., an aeolian dune field, or a part thereof).

Each depositional complex is divided into a series of architectural or geomorphic elements (Fig. 3; Fig. 4D). Architectural elements are defined as distinct sedimentary bodies with characteristic sedimentological properties (e.g., internal composition, geometry) and are the products of sediment accumulation in a specific sub-environment of deposition (e.g., a dune, a wet interdune, or a fluvial channel). Geomorphic elements are defined as modern landforms (or their remnants) present at the surface of the Earth, with distinctive physiographic characteristics; they are classified by sub-environment type (e.g., a linear dune, a star dune, a zibar, a sandsheet).

Both architectural and geomorphic elements can be subdivided further into facies elements (Fig. 3F; Fig. 4E). Facies elements are defined as sedimentary bodies that are distinguished from neighbouring sediments based on sediment composition, texture, structure, bedding geometry, fossil content, or by the nature of their bounding surfaces (Fig. 3F, 4E).

DASA records the hierarchical relationships between sedimentary units of different orders, ranging in broadly decreasing scale from depositional complexes, through architectural or geomorphic elements, to facies elements (Fig. 4). DASA records the containment of a lower-order (smaller-scale) element within a higher-order (larger-scale) element (e.g., nesting of a facies element within an architectural element; nesting of an architectural element within a depositional complex; Fig. 3). In parallel with this rigid hierarchy, DASA adopts an open hierarchy for certain units of the same rank: geomorphic, architectural and facies elements (cf. Colombera et al., 2016; Cullis et al., 2019). This allows hierarchical relationships between different units of the same rank to be stored, using parent-child relationships. This may be applicable, for example, where a dune set (child element) is present within a dune coset (parent element), or where a barchan dune (child element) occurs superimposed on a megadune or draa-scale bedform (parent element).

Hard data (e.g., quantitative measurements of element dimensions, grain-size statistics, petrophysical properties) stored in DASA are supplemented by soft (qualitative) data (e.g., interpretations of aeolian surface types, or facies element types). The types of data contained in each particular subset may vary markedly, depending on the manner by which the original data were collected and in terms of the hierarchical levels they cover. To assign a measure of quality to query outputs, data added to DASA are classified in terms of perceived quality (cf. Baas, 2005; Colombera et al., 2012a, 2016), based on three categories (‘A’, highest quality, to ‘C’ lowest quality) applied on the basis of expert judgement and quality criteria.

By utilizing this structure, DASA can effectively record all key aspects of aeolian sedimentology and stratigraphy. The different entity types recorded in DASA are outlined in some detail below. A full account of entity types (tables) and attributes (columns) can be found in Supplementary Information 1. DASA is a flexible and expandable system, which allows for the addition of new entity types (tables) or attributes (fields) for capturing other geological entities or variables of interest.

3.1 Table (Entity) Descriptions

3.1.1 Sources

The ‘sources’ table describes the primary source of the data. This table records (1) a full reference and (2) the data-source type (e.g., published literature, technical reports, unpublished academic work).

3.1.2 Case Studies

The ‘case studies’ table contains metadata (i.e., data that describe and give information about other data) relating to the geological background and geographical setting of each entry. Examples of the metadata stored in the ‘case studies’ table include: (1) chronostratigraphic information; (2) lithostratigraphic information; (3) the geographical location, a broad palaeogeographical location and dune-field name; (4) the basin name and basin type.

3.1.3 Subsets

In DASA, aeolian systems are subdivided into so-called subsets (cf. Colombera et al., 2012a) of a particular case study. Subsets are named or numbered depictions of collections of data within source material (Fig. 4A) and are differentiated on the basis of attributes that describe their geological boundary conditions or context, or because of their suitability to yield particular types of outputs. These attributes are reflected in the contents of the 'subset' table, which contains data describing the depositional system, its allogenic controls and metadata. Subsets are established to aid querying of the database on parameters that characterize depositional systems.

3.1.4 Subset Statistics

A table is included in DASA specifically for recording data presented as statistical summaries, which cannot therefore be assigned to a particular geological unit (e.g., a specific depositional complex, architectural element, geomorphic element or facies). Such data are instead stored as statistics for the entire subset. Examples of subset statistics include mean dune spacing, mean dune height, and mean wavelength and amplitude of dune along-crestline sinuosity.

3.1.5 Depositional Complexes

Subsets can be subdivided into depositional complexes, either on the basis of stratigraphic divisions (e.g., on a sedimentary graphic log; Fig. 3B) or in planform (e.g., on an aerial photograph). Depositional complexes are assigned a primary and – if appropriate – a secondary complex type; depositional complex types used in DASA are outlined in Table 3 and the application of a primary and secondary depositional complex type is illustrated in Fig. 4B-C. The terms 'primary' and 'secondary' qualify the relative dominance of different types of deposits of different origins within a subset. The primary depositional complex type defines the most abundant type of deposit in the unit (e.g., as a fraction of a stratigraphic log (Fig. 4B-C), or of a planform area); the secondary depositional complex type defines the second most common type. This approach enables recording the interaction between aeolian and non-aeolian systems, and facilitates database querying based on the sedimentary environment.

The ‘depositional complex’ table stores data on depositional complexes. Examples of attributes recorded in the ‘depositional complex’ table include: (1) dimensional parameters of the depositional complex; (2) whether the depositional complex is indicative of a dry, wet, mixed or stabilizing aeolian system (*sensu* Kocurek and Havholm, 1993); (3) whether the depositional complex has any recordable cyclicity (e.g., wetting- or drying-upward trends; George and Berry, 1993; Howell and Mountney, 1996); (4) the preservation mechanism of the depositional complex, for example via bedform climbing (Rubin and Hunter, 1982; Mountney, 2012), or via exceptional preservation following inundation by marine flooding (Glennie and Buller, 1983) or burial by extrusive igneous activity (Jerram et al., 1999, 2000a, 2000b; Mountney et al., 1999a; Mountney and Howell, 2000); and (5) for modern depositional complexes, the dominant wind direction and variability thereof (Fryberger, 1979).

3.1.6 Architectural and Geomorphic Elements

Depositional complexes can be subdivided into architectural or geomorphic elements (Fig. 3D; Fig. 4D), classified to cover the variety of aeolian and associated non-aeolian architectural and geomorphic element types that occur within aeolian systems (Table 4). In DASA, architectural elements describe the preserved 2D or pseudo-3D architectures of specific aeolian and associated non-aeolian elements.

Architectural elements may be used to describe properties of both ancient and recent deposits. The latter are recorded as architectural elements where the internal structures of modern dunes are revealed, for example, in trenches or by a ground penetrating radar (GPR) survey (Bristow et al., 2000b; Bristow, 2009; Tatum and Francke, 2012a, 2012b). In the ancient record, architectural elements are most commonly observed in outcrop, though are also recorded from some subsurface datasets, for example by using GPR (e.g., Jol et al., 2003; Bristow et al., 2005), by using seismic methods (e.g., Story, 1998), or by correlation of well logs (e.g., Strömbäck and Howell, 2002; Besly et al., 2018). In DASA, geomorphic elements describe the planform, 2D or 3D morphologies of landforms observed at the Earth's surface. DASA enables both the geomorphic expression and the deposit of an accretionary landform (e.g., a dune) to be recorded, respectively as geomorphic and architectural elements; this is applicable, for example, in cases where a dune is both viewed in planform in an aerial photograph (geomorphic element) and in cross section via dune trenching (architectural element) (e.g., McKee, 1966; Glennie, 1970, McKee and Moiola, 1975).

The open hierarchy of DASA enables architectural and geomorphic elements to be recorded in a way that reflects the hierarchy of sub-environments and/or of architectures they represent (e.g., cross-strata package within a dune set). This hierarchical arrangement is applied in the form of the relative containment of elements within other elements. In some cases, architectural-element boundaries may be ambiguous due to gradational element transitions between different sub-environment types. In DASA the boundaries of architectural elements are determined from the original source work (cf. Colombera et al., 2016).The employed data encoding methodology, as developed and refined by Colombera et al. (2016), provides a flexible approach to the subdivision of elements and allows DASA to be coded in a flexible manner. However, it should be noted that this approach nevertheless relies on the interpretations of architectural element boundaries as presented in the original sources.

The 'architectural element' and 'geomorphic element' tables contain primary data and metadata, including: (1) dimensional parameters; (2) element shapes and (3) element sub-environment classification (Table 4). Some additional parameters recorded for dune-set architectural elements, where appropriate, including foreset dips and azimuths, for example. For dune geomorphic elements, additional parameters are used, where appropriate, to record attributes such as the number of slipfaces, wavelength and amplitude of along-crestline sinuosity, and orientation relative to wind direction, and the lengths and angles of inclination of bedform stoss and lee slopes.

3.1.7 Facies Elements

The 'facies element' table contains primary data and metadata regarding the facies that comprise architectural and geomorphic elements, including: (1) dimensional parameters; (2) element shapes; and (3) types of facies (Table 5). Facies-element types are not mutually exclusive and cover deposits at different scales; this approach to classification was chosen because the database accommodates an open hierarchy of facies, implemented in the same manner as that outlined for geomorphic and architectural elements. A suite of further DASA parameters describing the lithology, grading and lamination types of facies elements are shown in Figure 4F, alongside parameters that describe post-depositional deformation (e.g., Rodríguez-López and Wu, 2020), including physical, chemical, biogenic and structural features.

3.1.8 Transitions Tables

Any element may transition to a different element belonging to the same order (e.g., the architectural-element order; Fig. 3H-K) vertically or laterally; lateral transitions can occur along a direction either parallel or perpendicular to the dominant foreset azimuth, else to indicators of the overall (palaeo)wind direction. Transition tables record the style of juxtaposition of neighbouring elements of the same order, and – where appropriate – the transitions between nested parent and child elements of the same order. Transitions between elements of the same scale may occur through bounding surfaces (see below). Additionally, gradational transitions may occur where no bounding surface is present (e.g., from deposits of a dry-interdune element upward into the toeset deposits of an overlying dune element).

3.1.9 Bounding Surfaces

Brookfield (1977) identified a hierarchy of bounding surfaces (third-, second- and first-order), and this classification scheme was later succeeded by nomenclature summarized by Kocurek (1996), which defined bounding-surface types of broadly equivalent status to those of Brookfield (1977): reactivation surfaces, superposition surfaces, interdune migration surfaces. In addition, a higher-order class of bounding surfaces is also adopted: the supersurface (Loope, 1985; Langford and Chan, 1988; Fryberger, 1993; Kocurek, 1988, 1996). Reactivation, superposition and interdune surfaces are chiefly the products of autogenic bedform migration; supersurfaces are chiefly the product of allogenic forcing (Fryberger, 1993) but can also potentially be generated by the regional migration of a major aeolian sand-sea (or erg) system (Porter, 1986).

The surface table records data on bounding surfaces, including the following: (1) the length, orientation and dip of the bounding surface; (2) association of features (sedimentary structures) indicative of substrate conditions (e.g., dry, damp, wet) associated with the surface; (3) association of features indicative of surface stabilization; (4) a classification of surface type (i.e., environmental significance) according to the schemes of Fryberger (1993) and Kocurek (1996); (5) a record of sedimentary structures associated with the surface, for example palaeosols, (Basilici et al., 2009; Dal' Bo et al., 2010), rhizoliths (Loope, 1988) and burrows (Ahlbrandt et al., 1978; Krapovickas et al., 2016), amongst others. A 'surfaces relationship' table is also present in DASA; this records any cross-cutting and truncation relationships between two surfaces.

3.1.10 Petrophysical and Textural Properties

Instances of geomorphic, architectural or facies elements (e.g., an interdune, or a sandsheet element) may be assigned specific petrophysical or textural properties; these data are recorded in the 'petrophysics' and 'texture' tables. The 'petrophysics' table records any petrophysical attributes of a given element, such as values of porosity and permeability. The 'texture' table records properties relating to grain character, including grain size, sorting and roundness.

4. DASA Output and Applications

At the time of writing, DASA contains data on 62 case studies: 28 case studies refer to modern aeolian systems (Table 1; Fig. 5); 34 case studies to ancient aeolian systems (Table 2; Fig. 5). DASA contains 252 subsets, 2631 architectural elements, 3651 geomorphic elements, 1321 facies elements, 2881 architectural-element transitions and 802 facies-element transitions. The application of DASA to fields of both fundamental and applied research in sedimentary geology relies on the collation of significant amounts of data; moreover, new datasets are being published frequently. As such, database population is ongoing and open-ended. Database outputs inevitably reflect the content of DASA at the time of database interrogation. If case-studies representing a particular geographic location (e.g., the Colorado Plateau) or a particular interval of geological time (e.g., Mesosozoic) are over-represented, DASA outputs will be biased accordingly. To mitigate such sampling biases, the case studies that have thus far been included in DASA have a global distribution and cover a wide span of geological time. Any sampling biases must however be considered when interpreting the significance of databaseoutputs.

Interrogation of DASA using SQL queries generates quantitative data outputs, which can be used to characterize the geomorphology and sedimentary architecture of modern and ancient aeolian systems, respectively. DASA queries can be tailored to deliver bespoke data outputs, based on the classification of the aeolian system (e.g., systems with damp interdunes, or systems characterized by drying-upward successions, or systems with an associated secondary depositional complex of lacustrine origin). Bespoke outputs can also be classified on metadata (e.g., only Mesozoic aeolian systems, studies based on GPR data, or studies from Arizona, USA). The ability to perform queries defined on multiple attributes (for example a specific geological age and a specific dune-field physiographic setting) enables the selection of data from multiple geological analogues that meet specific criteria. As such, quantitative data can be used to construct specialized bespoke models describing attributes of systems for which no single case-study example is wholly representative.

Outputs of DASA yield insights into the following: (1) the organization of aeolian systems and their constituent architectural and geomorphic building blocks; (2) the hierarchical containment relationships between elements of different scales; and (3) the distribution and spatial relationships between elements from the depositional-complex to the facies-element scale. Below, a series of example database outputs are presented to illustrate the value of DASA as a tool for the detailed characterization of aeolian sedimentary systems and their preserved successions. An SQL file containing the DASA database and all of the data used to generate the following figures are included in the supplementary information.

4.1 Comparison of Modern and Ancient Analogues

Understanding the relationship between modern and ancient aeolian systems remains important: modern aeolian systems are widely applied as analogues to help better understand the palaeoenvironmental significance of subsurface successions (e.g., Stanistreet and Stollhofen, 2002; Tatum and Francke, 2012a; Besly et al., 2018; Kocurek et al., 2020). In particular, compilations of cross-plots between dune height, length and width (e.g., Finkel, 1959; Long and Sharp, 1964; McKee, 1979; Wasson and Hyde, 1983; Bishop 1997; Lancaster, 2009; Bhadra et al., 2019) are a valuable tool for characterizing bedform relationships and understanding patterns of dune-field evolution. DASA provides a platform to reconcile such data from a wide variety of published sources, derived from original studies that considered different spatio-temporal settings and employed various methods of data collection. DASA captures data relating to both modern systems (i.e. geomorphic elements on the Earth's surface) and ancient successions (i.e. architectural elements preserved in the rock record), thereby providing a platform to make comparisons of the range of dimensions of modern forms and of their preserved counterparts in accumulated sedimentary successions.

DASA can be queried using nomenclature adopted in the original source work; for example, the designated dune type. Figure 6 shows a comparison of dune scaling relationships for modern dunes and ancient dune sets, which have been subdivided according to identified dune type. Measurements from modern dunes record the height, length and width of active bedforms at an instant in time. Measurements from accumulated dune sets record the dimensions of the preserved dune elements, which typically preserve only the lowermost parts of the original bedforms, and record the passage or migration of those bedforms over an extended episode of time (Rubin and

Hunter, 1982; Kocurek, 1991). As such, the preserved dimensions of dune sets are related in part to the geometries (e.g., the height, length, or width) and original morphologies of the bedforms that generated them, but also to the time interval over which the bedforms persisted, and the speed at which those bedforms migrated, together with other aspects of migratory behaviour, such as the angle of climb (Kocurek, 1991; Rubin, 1987; Rubin and Carter, 2006).

Scatter plots illustrate how different modern dune types have distinct scaling relationships (Fig. 6A-C); for example, modern parabolic dunes have the largest average height-to-length ratio of all dune types recorded in DASA (Fig. 6A). In the accumulated stratigraphic record, however, no clear relationship between inferred dune type and preserved set geometry is evident (Fig. 6D-F). Dune sets interpreted to represent accumulated deposits of the same fundamental dune type can take markedly different forms, with highly variable relationships between dune-set thicknesses, lengths and widths (Fig. 6D-F; cf. Bagnold 1941; Glennie 1970, Tsoar 1982; Kocurek, 1991; Romain and Mountney, 2014). Preserved dune-set scaling relationships (e.g., relationships between preserved dune-set thickness, length and width) are not necessarily strongly related to formative dune type.

This statement is based on the assumption that, in all source works, the original dune type was confidently interpreted from preserved dune sets; however, interpretations of formative dune type from evidence in the rock record are not always straightforward. For example, the preserved deposits of linear dunes can come to resemble those of crescentic dunes if the migrating bedforms undertook a component of lateral migration (Rubin and Hunter, 1985; Clemmensen, 1989; Rubin, 1990; Besly et al., 2018; Scotti and Veiga, 2019). The data presented in Figure 6A-F suggest either that dune type has no directly quantifiable relationship with the resulting preserved dune-set geometry, else that our ability to interpret and reconstruct dune types from evidence preserved in the ancient record is generally limited.

DASA also provides a unifying platform to directly compare modern and ancient systems, and to explain mechanisms of aeolian dune accumulation to form sets of strata. Direct comparisons of modern dune heights and ancient dune-set thicknesses (Fig. 6G-H) show that, for all dune types, modern bedform heights are typically an order of magnitude greater than the thicknesses of preserved dune sets. This finding is congruous with the idea that only a small portion of the original dune height is typically translated into the geological record and that dune-set deposition is the product of bedform climbing at low (i.e. subcritical) angles (Rubin and Hunter, 1982; Kocurek, 1981; Kocurek, 1991), whereby the rate of bedform migration was considerably greater than the rate of vertical accumulation (Kocurek, 1991).

In some instances dune bedform topography can be preserved in the geological record, to varying degrees, by geomorphic accommodation space where one set of bedforms generates topographic relief and where local accommodation in interdune depressions is subsequently filled by later bedforms (Langford et al., 2008; Fryberger and Hern, 2014; Kocurek et al., 2020). In other cases, dune bedform topography can be preserved by burial beneath extrusive volcanics (Clemmensen, 1988; Jerram et al., 1999, 2000a, 2000b; Scherer, 2000, 2002), or by marine inundation, or other sediments (Eshner and Kocurek, 1986, 1988; Fryberger, 1986; Chan and Kocurek, 1988; Strömbäck et al., 2005; Scotti and Veiga, 2019). Examples in which dune topography is fossilized in the geological record are recorded in DASA but are not depicted in Figure 6.

4.2 Characterization of Aeolian Architectural Elements

Architectural elements are the fundamental building blocks of aeolian sedimentary successions. DASA permits tailored querying to quantify the geometry of architectural elements from subsets classified according to boundary conditions, which may influence preserved aeolian architectures. Figure 7 illustrates an example of how filters might be applied to DASA to determine the relative dominance of particular aeolian architectural-element types through geological time, and for different palaeogeographic configurations. In the depicted example, the architectural elements are grouped according to four palaeogeographic settings associated with (1) the Proterozoic supercontinents (Rodinia and Columbia), (2) with Gondwanaland, (3) with Pangaea, and (4) with geological times characterized by dispersed continental landmasses for systems that developed since 38 Ma (Fig. 7A). The relative proportions of dune-set, sandsheet and interdune elements are plotted for the different settings (Fig. 7B-E), allowing an evaluation of the degree to which the global palaeogeographic configuration might have controlled the occurrence of aeolian successions characterized by particular architectural-element types. For example, sandsheet elements form a markedly greater proportion of Proterozoic aeolian systems (Fig. 7B), compared to all other settings (Fig. 7C-E): 34% compared to 15% in successions younger than 38 Ma (Fig. 7E). The relatively greater proportion of sandsheet elements in Proterozoic aeolian systems may reflect their increased prevalence prior to the evolution of land plants (e.g., Rainbird, 1992; Long, 2006; Davies and Gibling, 2010). The absence of the stabilizing effects of vegetation in Proterozoic settings likely promoted enhanced winnowing of fluvial braid plains to form aeolian sandsheet elements (e.g., Dott and Byers, 1981; Tirsgaard and Øxnevad, 1998; Erikkson and Simpson, 1998; Abrantes, 2020). The relatively lower proportion of sandsheet elements in aeolian systems younger than 38 Ma may reflect the stabilizing effects of grasses, which evolved between 60-55 Ma (Jacobs et al., 1999; Kellog, 2000), and which act to markedly retard aeolian winnowing, thereby reducing the supply of sediment suitable for sandsheet accumulation.

Proterozoic dune-set element thicknesses (median = 1.2 m) and sandsheet element thicknesses (median = 0.4 m) are markedly less than those of equivalent elements known from successions of the Gondawanan (dune set median thickness = 5 m; sandsheet median thickness = 2.0 m) and Pangaean (dune set median thickness = 2 m; sandsheet median thickness = 2.0 m) supercontinents (Fig. 7F and 7I-K). This may reflect the fact that the majority of Proterozoic successions are recorded from intracratonic basin settings, which are preferentially preserved in the central parts of stable ancient cratons (e.g., Shaw et al., 1991; Aspler and Chiarenzelli, 1997; Deb and Pal, 2015), and which typically experienced low rates of subsidence compared to other basin types (e.g., Bethke, 1985; Aspler and Chiarenzelli, 1997). This might have favoured the accumulation and preservation of relatively thin genetic aeolian units, in which aeolian dune-sets likely climbed at low-angles and accumulated sporadically between long episodes of sediment bypass under conditions of low rates of accommodation generation. Although the size of dune-sets could also be related the size of the formative dunes, this is not likely related to the effects of accommodation generation. The presence of vegetation in Gondwanan and Pangaean settings may have also acted to facilitate preservation of aeolian dune and sandsheet elements by limiting the mobility of river systems that could have wandered across and largely reworked aeolian sediments (Davis and Gibling, 2010; Reis et al., 2020). By contrast, Proterozoic fluvio-aeolian systems that lacked vegetated floodplains were instead more likely to be reworked by mobile rivers (Clemmensen and Dam, 1993; Aspler and

Chiarenzelli, 1997; Eriksson and Simpson, 1998; Els, 1998). Mixed fluvial-aeolian successions of Proterozoic age are typically only preserved where high water tables acted to retard and limit aeolian erosion (Trewin, 1993; Tirsgaard and Øxnevad, 1998).

Figure 7 shows just one example of how DASA can be used to determine the manner in which aeolian sub-environments variably develop and are preserved as a function of their specific spatio-temporal settings, possibly because of controls exerted by regional or global palaeogeographic configurations. Examples of other potential applications of this type of architectural-element characterisation are outlined below. (1) The compilation of foreset-azimuth data for specific supercontinental or basin settings; such datasets may be applied to aid the reconstruction of regional or localised paleowind directions (e.g. Bigarella and Salumni, 1961, 1964; Glennie, 1983; Parrish and Peterson, 1988; Scherer and Goldberg, 2007; Ballico et al., 2017; Scherer et al., 2020). (2) The compilation of architectural element data for specific paleoclimatological settings; such datasets may be applied to build quantitative facies models describing aeolian accumulation under icehouse and greenhouse climate conditions (e.g., Cosgrove et al., 2021)

4.3 Characterization of Aeolian Lithofacies

Aeolian lithofacies have variable sedimentological and petrophysical properties; understanding facies distribution, geometry and internal textural characteristics is important for gaining insight into depositional processes (Hunter, 1977). Figure 8 illustrates how DASA can be used to analyse quantitative facies metrics statistically, and to compare the geometries and grain-size characteristics of different aeolian facies. The ranges of thickness (Fig. 8B, C, E), length (Fig. 8B) and width (Fig. 8C), and the textural properties (Fig. 8D) of facies elements can be quantified and used in the generation of bespoke quantitative facies models. Database queries can be tailored to specific allogenic boundary conditions.

In Figure 9, three particular facies types are considered: (1) adhesion strata, (2) strata of interfingered grainflow, grainfall and/or wind-ripple origin, and (3) wind-ripple strata (Fig. 9A-C). DASA enables quantification of the architectures and of the sub-environments with which these facies are most closely associated (Fig. 9D-F). For example, it is possible to determine the proportions of the following: (1) adhesion strata that occur in damp and wet interdune environments (Fig. 9D); (2) interfingered strata that occur in aeolian dune environments (Fig. 9E), and wind-ripple strata that occur in sandsheet, or dry interdune, or water-table-influenced interdune settings (Fig. 9F).

The proportions of modal sand granulometric classes for the three example facies units are also shown (Fig. 9G-I); all facies types are dominated by fine- and medium-grained sand, which together form 91%, 75% and 65% of recorded modal grain sizes in adhesion strata, interfingered strata, and wind-ripple strata, respectively. This reflects the highly discriminant nature of sediment transport by the wind (Bagnold, 1941). Of note, the wind-ripple facies contains the largest proportions of coarse- and very coarse-grained sand (modal grain size in 33% of recorded instances). Coarse-grained wind-ripple deposits are especially common in aeolian sandsheet settings. This is notably the case for sandsheets that represent remnants of eroded landforms of original higher relief. The coarser grain-sizes found in sandsheet settings partly reflects the effects of aeolian deflation, whereby the winnowing of finer-grained sand leaves behind a coarser lag (Neilsen and Kocurek, 1986; Pye and Tsoar, 1990; Mountney and Russell, 2004, 2006; Mountney 2006b).

Quantitative output from DASA can be applied to elucidate understanding of the hierarchical arrangement, geometry and textural properties of a broad range of aeolian and associated non-aeolian facies types. The configuration of stratal packages comprising common aeolian facies (e.g., wind-ripple, grainfall and grainflow strata) can significantly impact horizontal and vertical permeability due to inter-facies variability in grain-size, sorting and packing (Hunter, 1977; Chandler et al., 1989; Prosser and Maskall, 1993). As such, DASA can be applied to better constrain facies-scale heterogeneity in aeolian reservoirs.

4.4 Element Transitions

The construction of meaningful facies models requires a quantitative understanding of the expected vertical arrangement and ordering (i.e. stacking) and lateral juxtaposition of elements. To this end, DASA can return statistics on transitions between elements of the same rank (e.g., depositional complexes and architectural and facies elements), and also between elements of different hierarchical scales (e.g., transitions from an underlying depositional complex of a given type to an overlying facies type, which is itself contained within a parent element of higher hierarchical order). The architectural, facies and textural information described in the examples presented above can be coupled with DASA outputs describing the mutual association of element types in lateral and vertical directions.

Figure 10 illustrates vertical transition statistics between types of architectural elements recorded in DASA. This type of information can be synthesized in transition probability matrices, in this example depicted as a heatmap (Figure 10D), or as stacked bar charts (Fig. 10E-F) to show the probability of transitioning from one element type to another. Specific architectural element types can be considered in terms of their probability or frequency of transition (vertically, or laterally along a direction either parallel or perpendicular to the dominant foreset azimuth) into another architectural-element type. This makes it possible, for example, to determine that: (1) aeolian sandsheet elements are most frequently seen to transition vertically to overlying dune sets (36% probability), or that (2) the probability of passing vertically from an aeolian dune set, below, directly to a non-aeolian architectural element above is 13% (Fig. 10E), and that this non-aeolian element has a 25% chance of being a fluvial channel deposit (Fig. 10F). Transition statistics can also be derived for facies and grain-size categories. These statistics can be used to characterize the internal facies organization of particular sub-environments and to quantify stratigraphic trends, through statistical evaluation (e.g. employing Markov-chain analysis; cf. Harper, 1984; Brierley, 1989) of the most likely vertical or lateral successions of facies elements. Understanding the vertical and lateral stacking (i.e. order of juxtaposition) of different element types is especially important in the interpretation of subsurface aeolian successions known only from core or wireline-log records (e.g., Chandler et al., 1989; Krystinik, 1990; Prosser and Maskall, 1993; Shebi, 1995; Besly et al. 2018).

4.5 Characterization of Aeolian Bounding Surfaces

Within aeolian systems, bounding surfaces separate elements at multiple scales and can demarcate prominent changes in sedimentological character. Such surfaces might signify the juxtaposition of separate aeolian sequences representing entirely different episodes of aeolian system construction and accumulation (e.g., Crabaugh and Kocurek, 1993), else they might record subtle changes between alternating episodes of dune accumulation via positive climb (e.g., Herries, 1993), non-climbing bypass (e.g. Langford and Chan, 1988), and erosion through negative climb (e.g., Kourek and Day, 2018; cf. Loope, 1985; Mountney, 2012).

DASA records both quantitative and qualitative data for all prominent surface types, and allows bespoke queries to be made on specific surface types and on any other higher-level filters. Two examples of how bounding-surface data can be sequentially filtered to meet particular specifications are shown in Figure 11A-B. Fig. 11A presents output on the percentage of supersurfaces (20% of all recorded bounding-surface types) that are Mesozoic in age (52% of supersurfaces), *and* that are wet (90% of Mesozoic supersurfaces), *and* that are bypass surfaces (48% of wet, Mesozoic supersurfaces). Fig. 11B presents output showing the percentage of interdune surfaces (50% of all recorded bounding-surface types) found at palaeolatitudes in the 15-30° range (42% of interdune surfaces), *and* that are curved in shape (54% of interdune surfaces from 15-30° latitude), *and* that are of a damp type (14% of curved interdune surfaces from 15-30° latitude). Such bespoke queries demonstrate the power of a databasing approach for enhancing our understanding of the timing and mechanism of preservation of surfaces of different types in the geological record, and of the characteristics that particular classes of bounding surface are likely to possess; such output can be used to build representative models of aeolian systems for different settings.

DASA can be applied to compare attributes of bounding surfaces of different order; examples of quantitative data output for the four main aeolian bounding-surface types (supersurfaces, and interdune migration, superposition and reactivation surfaces) are shown in Figure 12. Quantitative statistical summaries describing the lengths of different surface types, along directions that are both parallel and perpendicular to the azimuth of mean foreset dip in aeolian dune sets, are shown in Figure 12B-C; such statistical distributions of surface length can be used to guide stratigraphic correlations in aeolian successions, where limited exposure precludes direct walking-out of key stratal surfaces and across well arrays in the subsurface.

Data recorded in DASA reveal the following.

(1) Supersurfaces are twice more likely to be of deflationary type than of bypass type (Fig. 12D). Deflationary and bypass supersurfaces represent negative and neutral sediment budgets, respectively (Kocurek, 1988). The dominantly deflationary nature of supersurfaces is not surprising, as sustained sediment bypass (where dunes remain active but do not climb; e.g., Langford and Chan, 1988 requires sustaining a fine balance between sediment supply and downwind bedform migration. Under these conditions sediment supply is sufficient to maintain dune migration and to prevent dunes from cannibalizing their accumulation surface, but insufficient to promote the onset of bedform climbing (Mountney, 2012; “line of bypass” in his Figure 6).

(2) Supersurfaces are most likely to be associated with a ‘wet’ substrate (70%), compared to a ‘dry’ (10%) or ‘damp’ (20%) substrate (Fig. 12E). Such relations indicate the proximity of the water table at the time of supersurface development, which itself might be related to aeolian system interactions with adjoining fluvial and marine environments (Mountney et al., 1999b; Veiga et al., 2002; Scherer and Lavina, 2005, 2006; Scherer et al., 2007; Rodríguez-López et al., 2012; Basilici and Dal' Bo, 2014; Ferronatto et al., 2019; Reis et al., 2020).

(3) Twenty-five per cent of supersurfaces display evidence of surface stabilization, whereas 75% are unstabilized (Fig. 12F). Supersurfaces typically record substantial hiatuses in erg development and many are associated with sedimentary features indicative of long-term substrate stabilization, including rhizoliths, deflationary pebble lags and chemical cementation (Loope, 1985; Loope, 1988; Kocurek, 1991; Scherer

and Lavina, 2006; Basilici et al., 2009; Dal' Bo et al., 2010). However, such associated features are not ubiquitous and cannot be relied upon to assist in the identification of all supersurfaces. The lack of evidence for substrate stabilization for many supersurfaces may reflect the large time scales required for the development of some stabilizing features. For example, supersurfaces with abundant and prominent rhizoliths in the Permian Cedar Mesa Sandstone of Utah are thought to have taken 10^4-10^5 years to develop (Loope, 1985; Mountney, 2006a). The dominance of supersurfaces that lack evidence for significant substrate stabilization might indicate that resumption of aeolian accumulation prior to the development of stabilizing features was common in ancient systems. The lack of available tools with which to effectively date aeolian successions means that determining the length of time encapsulated by supersurfaces is, however, problematic. Additionally, the lack of stabilizing features may also reflect the prevailing climatic conditions. For example, the relatively rapid development of a protective mantle of vegetation is dependent on the establishment of relatively more humid climatic conditions; this may have been relatively rare in ancient systems preserved in the geological record.

(4) The substantial majority of supersurfaces (85%) have no appreciable relief and are classed as planar (Fig. 12G); this reflects their mode of formation over regional extents (Kocurek, 1991; Havholm et al., 1993); the majority of recorded supersurfaces are both deflationary and wet, and deflation to a “flat” regional water table would typically result in a planar surface (Stokes, 1968).

Bounding surfaces can potentially exert significant effects on reservoir heterogeneity due to the juxtaposition of facies of different lithologies and permeabilities; the lateral extent of facies-driven permeability contrasts across aeolian bounding surfaces can fundamentally influence fluid-flow in reservoirs where a facies unit on either side of the bounding surface has a permeability low enough to act to as baffle or barrier to fluid flow (Nagtegaal, 1979; Lindquist, 1983; Krystinik, 1990; Crabaugh and Kocurek, 1993; Herries, 1993; Shebi, 1995; Taggart et al., 2012). Additionally, the presence carbonate and siliceous cements on some bounding surfaces can generate low-permeability horizons within aeolian successions, which may be otherwise characterised by high net to gross ratios (Driese, 1985; Chandler et al., 1989; Kocurek and Havholm, 1993).

4.6 Creation of Quantitative Facies Models

DASA queries can be filtered to yield quantitative outputs on aeolian elements at multiple hierarchical orders, associated with different observational scales (Figs. 13 and 14). Two examples of how filters can be applied to DASA to produce bespoke quantitative aeolian facies models are outlined below.

To produce a facies model that quantifies architectural-element properties (Figure 13), filters can be applied in the following way.

(1) All recorded aeolian and non-aeolian architectural elements are considered according to their physiographic setting within a major aeolian sand sea (*sensu* Porter, 1986; Fig. 13A) to yield outputs on their geometric properties (Fig. 13B), and on their distribution within different dune-field settings (Fig. 13C).

(2) The properties of selected architectural-element types within a central-erg setting (Fig. 13D) are summarized; results demonstrate the relationships between recorded element length and thickness (Fig. 13E), and the range of recorded thicknesses, for these element types (Fig. 13F).

(3) An individual element type within a central-erg setting is considered (Fig. 13G). The thickness (Fig. 13H), length and width (Fig. 13I) of dune sets are reported.

(4) The internal properties of dune-set elements within central-erg settings are considered (Fig. 13J). Quantitative outputs (Fig. 13K-M) are reported, such as the relative proportions of single vs compound dune sets (Fig. 13M), the proportions of different facies type found in cross-bedded dune sets, and the proportions of different classes of modal sand grain-size (Fig. 13N-O).

To produce a facies model that quantifies facies properties of types of deposits (Figure 14), filters can be applied sequentially as follows.

(1) All recorded elements are considered according to depositional-complex type (Fig. 14A); the thickness distributions of all primary (Fig. 14B) and all secondary (Fig. 14C) depositional complex types are reported.

(2) The properties of architectural elements are filtered for a specific depositional-complex type, to characterize dune-set, sandsheet and interdune architectural elements from exclusively aeolian settings (Fig. 14D); the relationship between element lengths and thicknesses is reported (Fig. 14E), as are the thickness distributions of different element types (Fig. 14F).

(3) An individual architectural-element type present in aeolian systems is depicted; the element type is viewed in the context of its palaeogeographic and tectonic setting (Fig. 14G). In this example, interdunes are considered, for which thickness distributions are reported according to classes of supercontinental setting (Fig. 14H) and basin type (Fig. 14I).

(4) The facies properties of an individual element type are examined in the context of a specific supercontinental setting; in this case interdunes from Pangaea are considered. The proportion of dry, damp and wet interdune elements are reported (Fig.

14K), together with facies proportions shown for dry, damp, and wet interdunes (Fig. 14L-N).

The examples shown in Figures 13 and 14 demonstrate how outputs from DASA can be filtered from the scale of entire depositional systems representative of large-scale sedimentary environments (e.g., information regarding dune-field position or primary depositional complex type), down to the scale of individual lithofacies units (e.g., the facies and textural properties of particular types of bed sets). The examples described here merely depict a small number of filters that might be applied.

4.7 Characterizing Heterogeneities in Subsurface Aeolian Successions

The preceding examples illustrate how a database approach can be used to provide highly specific outputs based on particular sets of criteria. DASA can be applied as both a research tool to gain improved understanding of the controls that influence aeolian systems and their preserved successions, and as a resource to aid subsurface characterization The characterization of subsurface aeolian reservoirs requires the accurate determination of key reservoir parameters, including the lithology, geometry, dimensions and spatial distributions of aeolian, and associated non-aeolian elements (e.g., fluvial, playa-lake, and marine deposits, amongst others). Such key reservoir parameters can be determined from DASA output. Additionally. the synthesis of data from a large number of case studies permits the development of composite geological analogues that capture stratigraphic and sedimentological variability. These analogues can be applied to quantify uncertainty in subsurface aeolian successions Output from DASA can be applied, for example, in the fields of hydrocarbon exploration, development and production, carbon capture and storage (CCS), deep geothermal reservoir development, and in aquifer management (e.g., Medici et al., 2016, 2019a, 2019b). DASA can be used for a number of applied purposes, examples of which are as follows. First, to quantify the interdigitation and 3D stacking of relatively more porous and permeable aeolian dune elements (dominated by packages of grainflow strata) with non-dune elements (including interdune, fluvial and sabkha deposits) that tend to have poorer flow properties (cf. Fig. 10; Nagtegaal, 1979; Lindquist, 1983; Krystinik, 1990; Crabaugh and Kocurek, 1993; Herries, 1993; Shebi, 1995).

Second, to record the presence and nature of aeolian bounding surfaces at different scales, and their occurrence between and within specific depositional complexes and architectural and facies elements (Figs. 11 and 12). Aeolian bounding surfaces can act as barriers to fluid migration, by exhibiting prominent grain-size contrasts (e.g., Shebi, 1995; Ciftci et al., 2004). Bounding surfaces can also transmit percolating meteoric waters, resulting in the precipitation of carbonate and silicate cements (e.g., Chandler et al., 1989; North and Prosser, 1993), and in the acceleration of other diagenetic processes, such as the compaction and mechanical infiltration of clays and chlorite cementation (e.g., Bongiolo and Scherer, 2010; Dos Ros and Scherer, 2013).

Third, to characterize the statistically most likely configuration and orientation of aeolian facies units (e.g., Figs. 8 and 9), such as those composed of packages of wind-ripple, grainfall and grainflow strata. The three-dimensional arrangement of these aeolian facies elementscan significantly impact horizontal and vertical permeability due to inter-facies variability in grain size, sorting and packing (Hunter, 1977; Chandler et al., 1989; Prosser and Maskall, 1993; Howell and Mountney, 2001; Pickup and Hern, 2002).

Some aeolian successions have historically been considered to form relatively homogeneous tanks of sand due to inherent high net-to-gross ratios (e.g., Glennie, 1972). However, focused research has revealed many aeolian successions to be highly lithologically heterogeneous at multiple scales (e.g., McCaleb, 1979; Weber, 1987; Fryberger, 1990; Prosser and Maskall, 1993; Taggart et al., 2012; Godo, 2017). Such heterogeneity can be quantified by careful application of the database.

Aeolian successions are shown here to exhibit complex architectural arrangements of aeolian and associated non-aeolian elements, and to be lithologically heterogeneous, across a variety of scales (cf. McCaleb, 1979; Weber, 1987; Prosser and Maskall, 1993; Godo, 2017). Composite analogues derived from DASA can be employed as quantitative facies models (cf. Colombera et al., 2013), applicable (1) to predict three-dimensional lithological heterogeneity in subsurface successions that are resource targets; (2) to constrain geocellular stochastic models (cf. Enge et al., 2007; Colombera et al., 2012b; Howell et al., 2014), and (3) to facilitate borehole correlations of aeolian dune sets or associated non-aeolian elements (e.g., Lallier et al., 2012; Colombera et al., 2014).

5. Conclusions

DASA is the first integrated large-scale relational database specifically designed to store quantitative data on the geomorphology, sedimentology and stratigraphy of modern and ancient aeolian systems, and their preserved successions. The flexible structure of DASA and the associated standardization of data types and terminology allow the synthesis of data from multiple sources (e.g., published and unpublished literature, technical reports and bespoke studies), of different types (e.g., modern vs ancient; outcrop vs subsurface), and collected using different methods (e.g., vertical measured sections, architectural correlation panels, and virtual outcrop models).

DASA has been designed to capture all the fundamental attributes of aeolian architecture, including but not limited to: (1) the geometric properties of aeolian and associated non-aeolian bodies; (2) the spatial configuration of aeolian and related sedimentary and geomorphic units, including their vertical and lateral transitions; and (3) the nature of bounding surfaces that separate aeolian and non-aeolian bodies. Quantitative data incorporated within DASA are supported by associated qualitative data, including metadata describing age, location and broader environmental setting, together with information relating to original descriptions, interpretations and classifications of forms and deposits. Data on geological boundary conditions, such as tectonic setting and climatic conditions, are also stored to frame aeolian systems in time and space.

The digitization of aeolian architecture allows DASA to output quantitative metrics that span multiple scales, from larger-scale depositional complexes to smaller-scale facies elements and sediment texture. Tailored quantitative outputs describing aeolian architectures can be filtered to enable comparisons between aeolian systems deposited under different boundary conditions. Some potential applications of DASA to future research developments in aeolian sedimentology and stratigraphy include: (1) the development of quantitative facies models, specifically tailored for parameters describing spatio-temporal and environmental context; (2) the instruction of forward stratigraphic models and 3D geocellular subsurface models; and (3) the empirical assessment of how aeolian systems respond to – and how associated architectures record – allogenic and autogenic forcings. DASA serves as a valuable tool for quantitative subsurface characterization.

Data population is on-going as more studies of aeolian systems are published. The database-informed approach to research that DASA enables has the potential to revolutionize our understanding of processes and controls on aeolian sedimentary systems, both modern and ancient.

Data Availability Statement

An SQL file containing all of the data presented in this paper are available and included in the supplementary information.

Acknowledgements

We thank the sponsors and partners of FRG-ERG for financial support for this research: AkerBP, Areva (now Orano), BHPBilliton, Cairn India (Vedanta), CNOOC, ConocoPhillips, Chevron, Equinor, Murphy Oil, Occidental, Petrotechnical Data Systems, Saudi Aramco, Shell, Tullow Oil, Woodside and YPF. Claiton Scherer and an anonymous reviewer are thanked for their constructive comments.

References

Abrantes, F.R., Basilici, G. and **Soares, M.V.T**. (2020) Mesoproterozoic erg and sand sheet system: Architecture and controlling factors (Galho do Miguel Formation, SE Brazil). *Precam. Res.*, 338, 105592.

Ahlbrandt, T.S., Andrews, S. and **Gwynne, D.T.** (1978) Bioturbation in eolian deposits. *J. Sed. Petrol.*, 48, 839–848.

Al-Masrahy, M.A. and **Mountney, N.P.** (2013) Remote sensing of spatial variability in aeolian dune and interdune morphology in the Rub' Al-Khali, Saudi Arabia. *Aeolian Res.*, 11, 155-170.

Al-Masrahy, M.A. and **Mountney, N.P.** (2015) A classification scheme for fluvial–aeolian system interaction in desert-margin settings. *Aeolian Res.*, 17, 67–88.

Allen, J.R.L. (1963) The classification of cross-stratified units. With notes on their formation. *Sedimentology,* 2, 93-114.

Allen, J.R.L. (1978) Studies in fluviatile sedimentation: an exploratory quantitative model for the architecture of avulsion-controlled alluvial suites. *Sed. Geol.,* 21, 129-147.

Aspler, L.B. and **Chiarenzelli, J.R.** (1997) Initiation of 2.45–2.1 Ga intracratonic basin sedimentation of the Hurwitz Group, Keewatin Hinterland, Northwest Territories, Canada. *Precam. Res.*, 81, 265-297.

Baas, J.H., McCaffrey, W.D. and **Knipe, R.J.** (2005) The deep-water architecture knowledge base: towards an objective comparison of deep-marine sedimentary systems. *Petrol. Geosci.*, 11, 309–320.

Baitis, E., Kocurek, G., Smith, V., Mohrig, D., Ewing, R.C. and **Peyret, A.-P.B.** (2014) Definition and origin of the dune-field pattern at White Sands, New Mexico. *Aeolian Res.*, 15, 269-287.

Bagnold, R.A. (1941) The Physics of Blown Sand and Desert Dunes: London, Methuen & Company, 265 p.

Ballico, M.B., Scherer, C.M.S., Mountney, N.P., Souza, E.G., Chemale, F., Pisarevsky, S.A. and **Reis A.D.** (2017) Wind-pattern circulation as a palaeogeographic indicator: Case study of the 1.5-1.6 Ga Mangabeira Formation, Sao Francisco Craton, Northeast Brazil. *Precam. Res.*, 298, 1-15.

Banham, S.G., Gupta, S., Rubin, D.M., Watkins, J.A., Sumner, D.Y., Edgett, K.S., Grotzinger, J.P., Lewis, K.W., Edgar, L.A., Stack-Morgan, K.M., Barnes, R., Bell, J.F., III, Day, M.D., Ewing, R.C., Lapotre, M.G.A., Stein, N.T., Rivera-Hernandez, F. and **Vasavada, A.R.** (2018) Ancient Martian aeolian processes and palaeomorphology reconstructed from the Stimson formation on the lower slope of Aeolis Mons, Gale crater, Mars. *Sedimentology*, 65, 993-1042.

Bart, H.A. (1977) Sedimentology of cross-stratified sandstones in Arikaree Group, Miocene, Southeastern Wyoming. *Sed. Geol.*, 19, 165-184.

Basilici, G. and **Dal' Bo, P.F.F.** (2014) Influence of subaqueous processes on the construction and accumulation of an aeolian sand sheet. *Ear. Surf. Proc. Landf.,* 39, 1014-1029.

Basilici, G., Dal' Bo, P.F.F. and **Ladeira, F.S.B.** (2009) Climate-induced sediment-palaeosol cycles in a Late Cretaceous dry aeolian sand sheet: Marília Formation (North-West Bauru Basin, Brazil). *Sedimentology*, 56, 1876-1904.

Bateman, M.D., Holmes, P.J., Carr, A.S., Horton, B.P. and **Jaiswal, M.K.** (2004) Aeolianite and barrier dune construction spanning the last two glacial-interglacial cycles from the southern Cape coast, South Africa. *Quatern. Sci. Rev.*, 23, 1681-1698.

Benan, C.A.A. and **Kocurek, G.** (2000) Catastrophic flooding of an aeolian dune field: Jurassic Entrada and Todilto Formations, Ghost Ranch, New Mexico, USA. *Sedimentology*, 47, 1069-1080.

Besly, B., Romain, H.G. and **Mountney, N.P.** (2018) Reconstruction of linear dunes from ancient aeolian successions using subsurface data: Permian Auk Formation, Central North Sea, UK. *Mar. Pet. Geol.,* 91, 1-18.

Bethke, C.M. (1985) A numerical model of compaction-driven groundwater flow and heat transfer and its application to the paleohydrology of intracratonic sedimentary basins. *J. Sol. Ear.,* 90, 6817-6828.

Beveridge, C., Kocurek, G., Ewing, R., Lancaster, N., Morthekai, P., Singhvi, A. and **Mahan, S.** (2006) Development of spatially diverse and complex dune-field patterns: Gran Deserierto Dune Field, Sonora, Mexico. *Sedimentology*, 53, 1391-1409.

Bhadra, B.K., Rehpade, S.B., Meena, H. and **Rao S.S**. (2019) Analysis of parabolic dune morphometry and its migration in Thar Desert area, India, using high-resolution satellite data and temporal DEM. *J. Indian. Soc. Rem. Sens.*, 47, 2097-2111.

Bigarella, J.J. and **Salamuni, R.** (1961) Early Mesozoic wind patterns as suggested by dune bedding in the Botucatu sandstone of Brazil and Uruguay. *Geol. Soc. Am. Bull.*, 72, 1089-1106.

Bigarella, J.J. and **Salamuni, R.** (1964) Palaeowind patterns in the Botucatu sandstone (Triassic-Jurassic) of Brazil and Uruguay. In: Problems in palaeoclimatology (Ed A.E.M. Nairn), Proceedings of the NATO, Palaeoclimates Conference held at the University of Newcastle upon Tyne, January 7-12, 1963, London: Interscience, pp. 406-409.

Bishop, M.A. (1997) The spatial and temporal geomorphology and surficial sedimentology of the Gurra Gurra crescentic dunes, Strzelecki Desert, South Australia. Unpublished PhD Thesis, University of Adelaide, Department of Geology and Geophysics.

Biswas, A. (2005) Coarse aeolianites: sand sheets and zibar-interzibar facies from the Mesoproterozoic Cuddapah Basin, India. *Sed. Geol*. 174, 149-160.

Blakey, R.C., Havholm, K.G. and **Jones, L.S.** (1996) Stratigraphic analysis of eolian interactions with marine and fluvial deposits, middle Jurassic Page Sandstone and Carmel Formation, Colorado Plateau, U.S.A*. J. Sed. Res.,* 66, 324–342.

Bongiolo, D.E. and **Scherer, C.M.S.** (2010) Facies architecture and heterogeneity of the flu-vialeaeolian reservoirs of the Sergi formation (upper Jurassic), Recôncavo basin, NE Brazil. M*ar. Pet. Geol.,* 27, 1885–1897.

Bourke, M.C., Ewing, R.C., Finnegan, D. and **McGowan, H.A.** (2009) Sand dune movement in the Victoria Valley, Antarctica. *Geomorphology*, 109, 148-160.

Brierley, G.J. (1989) River planform facies models: the sedimentology of braided, wandering and meandering reaches of the Squamish River, British Columbia. *Sed. Geol.,* 61, 17-35.

Bristow, C.S. (2009) Ground penetrating radar in Aeolian dune sands. In: *Ground Penetrating Radar: theory and applications* (Ed. H.M. Jol). pp. 273-297, Elsevier Science.

Bristow, C.S. and **Mountney, N.P.** (2013) Aeolian Landscapes, Aeolian Stratigraphy. In: *Treatise on Geomorphology* (Ed. J. Shroder), pp. 246-268. Elsevier, San Diegeo, USA

Bristow, C.S., Bailey, S.D. and **Lancaster, N.** (2000a) The sedimentary structure of linear sand dunes. *Nature*, 406, 56-59.

Bristow, C.S., Chroston, P.N. and **Bailey, S.D.** (2000b) The structure and development of foredunes on a locally prograding coast: insights from ground-penetrating radar surveys, Norfolk, UK. *Sedimentology*, 47, 923-944.

Bristow, C.S., Lancaster, N. and **Duller, G.A.T.** (2005) Combining ground penetrating radar surveys and optical dating to determine dune migration in Namibia. *J. Geol. Soc. London*, 162, 315–321.

Brookfield, M.E. (1977) The origin of bounding surfaces in ancient aeolian sandstones. *Sedimentology*, 24, 303-332.

Brookfield, M.E. (1992) Eolian systems. In: *Facies Models. Response to Sea Level Change* (Eds R.G. Walker, R.G and N.P. James*), Geol. Ass. Canada.*, pp. 143–156.

Cather, S.M., Connell, S.D., Chamberlin, R.M., McIntosh, W.C., Jones, G.E., Potochnik, A.R., Lucas, S.G. and **Johnson, P.S.** (2008) The Chuska erg: Paleogeomorphic and paleoclimatic implications of an Oligocene sand sea on the Colorado Plateau. *Geol. Soc. Am. Bull.*, 120, 13-33.

Chan, M.A. and **Kocurek, G.** (1988) Complexities in eolian and marine interactions: processes and eustatic controls on erg development. *Sed. Geol.*, 56, 283-300.

Chandler, M.A., Kocurek, G., Goggin, D.J. and **Lake, L.W.** (1989) Effects of stratigraphic heterogeneity on permeability in eolian sandstone sequences, Page Sandstone, northern Arizona. *Am. Assoc. Petrol. Geol. Bull.* 73, 658-668.

Chrintz, T. and **Clemmensen, L.B.** (1993) Draa reconstruction, the Permian Yellow Sands, northeast England. In: *Aeolian sediments. Ancient and modern* (Eds K. Pye and N. Lancaster). *Int. Assoc. Sedimentol. Spec. Publ.*, **16**, 151-161.

Ciftci, B. N., Aviantara, A.A., Hurley, N.F. and **Kerr, D.R.** (2004) Outcrop-based three-dimensional modeling of the Tensleep Sandstone at Alkali Creek, Bighorn Basin, Wyoming. In: *Integration of outcrop and modern analogues in reservoir modelling* (Eds G. M. Grammer, P. M. Harris, and G. P. Eberli) *Am. Assoc. Petrol. Geol. Mem.*, 80, p. 235–259.

Clemmensen, L.B. (1985) Desert sand plain and sabkha deposits from the Bunter Sandstone formation (L. Triassic) at the northern margin of the German Basin. *Geol. Rundsch.*, 74, 519-536.

Clemmensen, L.B. (1987) Complex star dunes and associated aeolian bedforms, Hopeman Sandstone (Permo-Triassic), Moray Firth Basin, Scotland. In: *Desert Sediments: Ancient and Modern* (Eds L.E. Frostick and I. Reid), *Geol. Soc. London Spec. Publ.*, 35, 213-231.

Clemmensen, L.B. (1988) Aeolian morphology preserved by lava cover, the Precambrian Mussartut Member, Eriksfjord Formation, South Greenland. *Bull. Geol. Soc. Denmark*, 37, 105-116.

Clemmensen, L.B. (1989) Preservation of interdraa and plinth deposits by lateral migration of large linear draa (Lower Permian Yellow Sands, northeast England). S*ed. Geol.*, 65, 139–151.

Clemmensen, L.B. and **Abrahamsen, K.** (1983) Aeolian stratification and facies association in desert sediments, Arran basin (Permian), Scotland. *Sedimentology*, 30, 311-339.

Clemmensen, L.B. and **Dam, G.** (1993) Aeolian sand-sheet deposits in the Lower Cambrian Neksø Sandstone Formation, Bornholm, Denmark: sedimentary architecture and genesis. *Sed. Geol.*, 83, 71-85.

Codd, E.F. (1970) A Relational Model of Data for Large Shared Data Banks. *Communications of the ACM*., 13, 377–387.

Cojan, I. and **Thiry, M.** (1992) Seismically induced deformation structures in Oligocene shallow-marine and aeolian coastal sands (Paris Basin). *Tectonophysics*, 206, 78-89.

Colombera, L., Mountney, N.P. and **McCaffrey, W.D.** (2012a) A relational database for the digitization of fluvial architecture concepts and example applications. *Petrol. Geosci*. 18, 129-140.

Colombera, L., Felletti, F., Mountney, N. P. and **McCaffrey, W. D.** (2012b). A database approach for constraining stochastic simulations of the sedimentary heterogeneity of fluvial reservoirs. *Am. Assoc. Petrol. Geol. Bull.*, 96, 2143-2166.

Colombera, L., Mountney, N.P. and **McCaffrey, W.D.** (2013) A quantitative approach to fluvial facies models: methods and example results. *Sedimentology*, 60, 1526-1558.

Colombera, L., Mountney, N. P., Felletti, F. and **McCaffrey, W. D.** (2014). Models for guiding and ranking well-to-well correlations of channel bodies in fluvial reservoirs. *Am. Assoc. Petrol. Geol. Bull.*, 98, 1943-1965.

Colombera, L., Mountney, N.P., Hodgson, D.M. and **McCaffrey, W.D.** (2016) The Shallow-Marine Architecture Knowledge Store: A database for the characterization of shallow-marine and paralic depositional systems. *Mar. Pet. Geol.*, 75, 83-99.

Cosgrove, G.I.E., Colombera, L. and **Mountney, N.P.** (2021) Quantitative analysis of the sedimentary architecture of eolian successions developed under icehouse and greenhouse climatic conditions. *GSA Bull.*, *In Press.*

Cowan, G. (1993) Identification and significance of aeolian deposits within the dominantly fluvial Sherwood Sandstone Group of the East Irish Sea Basin UK. In: *Characterization of Fluvial and Aeolian Reservoirs* (Eds C.P. North and D.J. Prosser), *Geol. Soc. Spec. Pub.*, 73, 231-245.

Crabaugh, M. and **Kocurek, G.** (1993) Entrada Sandstone: an example of a wet aeolian system. In: *The Dynamics and Environmental Context of Aeolian Sedimentary Systems* (Ed. K. Pye), *Geol. Soc. Spec. Pub.* 72, 105-126.

Cullis, S., Patacci, M., Colombera, L., Bührig, L. and **McCaffrey, W.D.** (2019) A database solution for the quantitative characterisation and comparison of deep-marine siliciclastic depositional systems, *Mar. Pet. Geol.*, 102, 321-339.

Dal' Bo, P.F.F., Basilici, G. and **Angélica, R.S.** (2010) Factors of paleosol formation in a Late Cretaceous eolian sand sheet paleoenvironment, Marília Formation, Southeastern Brazil. *Palaeogeog., Palaeoclim., Palaeoecol.,* 292, 349-365.

Dasgupta, P.K., Biswas, A. and **Mukherjee, R.** (2005) Cyclicity in Palaeoproterozoic to Neoproterozoic Cuddapah Supergroup and its significance in basinal evolution. In: *Cyclic Development of Sedimentary Basins* (Eds J.M. Mabesoone and V.H. Neumann), *Developments in Sedimentology*, 57, 313-354.

Davies, N.S. and **Gibling, M.R.** (2010) Cambrian to Devonian evolution of alluvial systems: The sedimentological impact of the earliest land plants. *Ear. Sci. Rev.*, 98, 171-200.

Deb, M. and **Pal, T.** (2015) Mineral potential of Proterozoic intracratonic basins in India. In: *Precambrian Basins on India* (Eds R. Mazumder and P.G. Eriksson), *Geol. Soc. London, Mem.*, 43, 309-325.

Derickson, D., Kocurek, G., Ewing, R.C. and **Bristow, C.S.** (2008) Origin of a complex and spatially diverse dune-field pattern, Algodones, southeastern California. *Geomorphology*, 99, 186-204.

De Ros, L.F. and **Scherer, C.M.** (2013) Stratigraphic Controls on the Distribution of Diagenetic Processes, Quality and Heterogeneity of Fluvial-Aeolian Reservoirs from the Recôncavo Basin, Brazil. In: *Linking Diagenesis to Sequence Stratigraphy* (Eds S. Morad, J.M. Ketzer and L.F. De Ros), John Wiley and Sons, New Jersey, USA, pp. 105–132

Dias, K.D.N. and **Scherer, C.M.S.** (2008) Cross-bedding set thickness and stratigraphic architecture of aeolian systems: An example from the Upper Permian Piramboia Formation (Parana Basin), southern Brazil. *J. S. Am. Ear. Sci.*, 25, 405-415.

Dong, Z., Wang, X. and **Chen, G.** (2000) Monitoring sand dune advance in the Takliman Desert, *Geomorphology*, 35, 219-231.

Dong, Z., Wei, Z., Qian, G., Zhang, Z., Luo, W. and **Hu, G.** (2010) "Raked" linear dunes in the Kumtagh Desert, China. *Geomorphology*, 123, 122-128.

Dott, R.H. and **Byers, C.W.** (1981) SEPM research conference on modern shelf and ancient cratonic sedimentation - the orthoquartzite-carbonate suite revisited. *J. Sed. Petrol.*, 51, 329-347.

Dott, R.H., Byers, C.W., Fielder, G.W., Stenzel, S.R. and **Winfree, K.E.** (1986) Aeolian to marine transition in Cambro-Ordovician cratonic sheet sandstones of the northern Mississippi valley, U.S.A. *Sedimentology,* 33, 345-367.

Driese, S.G. and **Dott, R.H., Jr** (1984) Model for sandstone carbonate ‘‘cyclothems’’ based on upper Member of Morgan Formation (Middle Pennsylvanian) of northern Utah and Colorado. *Am. Assoc. Petrol. Geol. Bull.,* 68, 574–597.

Elbelrhiti, H., Andreotti, B. and **Claudin P.** (2008) Barchan dune corridors: Field characterization and investigation of control parameters. *J. Geophys. Res*., 113. F02S15(F2).

Ellis, D. (1993) The Rough Gas Field: distribution of Permian aeolian and non-aeolian reservoir facies and their impact on field development. *Geol. Soc. Spec. Pub*., 73, 265-277.

Els, B.G. (1998) The auriferous late Archaean sedimentation systems of South Africa: unique palaeo-environmental conditions. *Sed. Geol.,* 120, 205-224.

Enge, H.D., Buckley, S.J., Rotevatn, A. and **Howell, J.A.** (2007) From outcrop to reservoir simulation model: Workflow and procedures. *Geosphere,* 3, 469-490.

Eriksson, P.G. and **Simpson, E.L.** (1998) Controls on spatial and temporal distribution of Precambrian eolianites. *Sed. Geol.*, 120, 275-294.

Eschner, T.B. and **Kocurek, G.** (1986) Marine destruction of eolian sand seas: Origin of mass flows. *J. Sed. Res.,* 56, 401-411.

Eschner, T.B. and **Kocurek, G.** (1988) Origins of relief along contacts between eolian sandstones and overlying marine strata. *Am. Assoc. Petrol. Geol. Bull.*, 72, 923-949.

Evans, G., Kendall., C.G.St.C. and **Skipwith, P.** (1964) Origin of coastal flats, the sabkha of the Trucial Coast, Persian Gulf, *Nature,* 202, 759-761.

Ewing, R.C. and **Kocurek, G.** (2010) Aeolian dune interactions and dune-field pattern formation: White Sands Dune Field, New Mexico. *Sedimentology*, 57, 1199-1219.

Finkel, H.J. (1959) The barchans of Southern Peru. *J. Geol.*, 67, 614-647.

Formolo Ferronatto, J.P., dos Santos Scherer, C.M.S, de Souza, E.G, dos Reis, A.D. and **de Mello, R.G.** (2019) Genetic units and facies architecture of a Lower Cretaceous fluvial-aeolian succession, Sao Sebastiao Formation, Jatoba Basin, Brazil. *J. S. Am. Ear. Sci.*, 89, 158-172.

Fryberger, S. G. (1986) Stratigraphic traps for petroleum in wind-laid rocks. *Am. Assoc. Petrol. Geol. Bull.*, 70, 1765-76.

Fryberger, S.G. (1990) Role of water in eolian deposition. In: *Modern and Ancient Eolian Deposits: Petroleum Exploration and Production* (Eds S.G. Fryberger, L.F. Krystinik and C.J. Schenk), *SEPM, Denver,* p. 1-11.

Fryberger, S.G. (1993) A review of aeolian bounding surfaces, with examples from the Permian Minnelusa Formation, USA. In: *Characterization of fluvial and aeolian* *reservoirs* (Eds C.P. North and D.J. Prosser), *Geol. Soc. London Spec. Publ.,* 73, 167-197.

Fryberger, S.G. and **Hern, C.Y.** (2014) A Geometric Approach to the Analysis of Global Eolian Hydrocarbon Reservoirs. *Am. Ass. Pet. Geol.,* Search and Discovery Article 41478

Fryberger, S.G. and **Schenk, C.J.** (1988) Pin stripe lamination- a distinctive feature of modern and ancient eolian sediments. *Sed. Geol.,* 55, 1-15.

García-Hidalgo, J.F., Temiño, J. and **Segura, M.** (2002) Holocene eolian sediments on the southern border of the Duero Basin (Spain): origin and development of an eolian system in a temperate zone. *J. Sed. Res.,* 72, 30-39.

George, G.T. and **Berry, J.K** (1993) A new lithostratigraphy and depositional model for the upper Rotliegend of the UK sector of the southern North Sea. In: *Characterization of fluvial and aeolian reservoirs* (Eds C.P. North and D.J. Prosser), *Geol. Soc. London Spec. Publ.*, 73, 291-319.

Gibling, M.R. (2006) Width and thickness of fluvial channel bodies and valley fills in the geological record: a literature compilation and classification. *J. Sed. Res.*, 76, 731–770.

Glennie, K.W. (1970) Desert Sedimentary Environments, In: *Developments in Sedimentology*, Elsevier, Amsterdam, 14, p.83.

Glennie, K.W. (1972) Permian Rotliegendes of Northwest Europe interpreted in the light of modern desert sedimentation studies. *Am. Assoc. Petrol. Geol. Bull.*, 56, 1048-1071.

Glennie, K.W. (1983) Early Permian (Rotliegendes) palaeowinds of the North Sea. *Sed. Geol.*, 34, 245-265.

Godo, T. (2017) The Appomattox field: Norphlet Aeolian sand dune reservoirs in the deep-water Gulf of Mexico. In: *Giant Fields of the Decade 2000–2010* (Eds R. K. Merrill, C. A. Sternbach). *Am. Assoc. Petrol. Geol. Mem.*, 113, 29-54.

Grotzinger, J.P., Arvidson, R.E., Bell, J.F., Calvin, W., Clark, B.C., Fike, D.A., Golombek, M., Greeley, R., Haldemann, A., Herkenhoff, K.E., Jolliff, B.L., Knoll, A.H., Malin, M., McLennan, S.M., Parker, T., Soderblom, L., Sohl-Dickstein, J.N., Squyres, S.W., Tosca, N.J. and **Watters, W.A.** (2005) Stratigraphy and sedimentology of a dry to wet eolian depositional system, Burns formation, Meridiani Planum, Mars. *Earth Planet. Sci. Lett.*, 240, 11–72.

Hamdan, M.A., Refaat, A.A. and **Abdel Wahed, M.** (2016) Morphologic characteristics and migration rate assessment of barchan dunes in the Southeastern Western Desert of Egypt. *Geomorphology*, 257, 57-74.

Harper, C.W. (1984) Improved methods of facies sequence analysis. In: *Facies Models* (Ed. R.G. Walker), 2nd edn, pp.11-13, Geoscience Canada Reprint Series no. 1.

Havholm, K.G., Blakey, R.C., Capps, M., Jones, L.S., King, D.D. and **Kocurek, G.** (1993) Aeolian genetic stratigraphy: an example from the Middle Jurassic Page sandstone, Colorado Plateau. In: *Aeolian sediments: ancient and modern* (Eds K. Pye and N. Lancaster). *Int. Assoc. Sedimentol. Spec. Publ.*, 16, 87-108.

Herries, R. D. (1993) Contrasting styles of fluvial-eolian interaction at a downwind erg margin: Jurassic Kayenta-Navajo transition, northeastern Arizona, U.S.A. In: *Characterization of fluvial and eolian reservoirs* (Eds C.P. North and D.J. Prosser), , *Geol. Soc. Spec. Publ.*, 73, p. 199–218.

Holz, M., Soares, A.P. and **Soares, P.C.** (2008) Preservation of aeolian dunes by pahoehoe lava: An example from the Botucatu Formation (Early Cretaceous), Mato Grosso do Sul state (Brazil), western margin of the Parana Basin in South America. *J. S. Am. Earth Sci.*, 25, 398-404.

Howell, J.A. and **Mountney, N.P.** (2001) Aeolian grain flow architecture: hard data for reservoir models and implications for red bed sequence stratigraphy. *Petrol. Geosci.*, 7**,** 51-56.

Howell, J.A., Martinius, A.W. and **Good, T.R.** (2014) The application of outcrop analogues in geological modelling: a review, present status and future outlook. In:

Sediment-Body Geometry and Heterogeneity (Eds A. W. Martinius, J. A. Howell and T.R. Good), *Geol. Soc. Lon. Spec. Pub.*, 387, 1-25.

Hummel, G. and **Kocurek, G.** (1984) Interdune areas of the Back-Island dune field, North Padre-Island, Texas. *Sed. Geol.*, 39, 1-26.

Hunter, R.E. (1977) Basic types of stratification in small eolian dunes. *Sedimentology*, 24, 361–387.

Hunter, R.E. (1981) Stratification styles in eolian sandstones: Some Pennsylvanian to Jurassic examples from the western interior USA. In: *Recent and Ancient Non-Marine Depositional Environments, Models for Exploration* (Eds F.G. Ethridge and R.M. Flore), *SEPM Spec. Publ.*, 31, 315-329.

Irmen, A.P. and **Vondra, C.F.** (2000) Aeolian sediments in lower to middle (?) Triassic rocks of central Wyoming. *Sed. Geol.*, 132, 69-88.

Jacobs, B.F., Kingston, J.D. and **Jacobs, L.L.** (1999) The origin of grass-dominated ecosystems. *Ann. Missouri Bot. Gard.*, 86, 590–643.

Jerram, D.A., Mountney, N.P., Holzforster, F. and **Stollhofen, H.** (1999) Internal stratigraphic relationships in the Etendeka Group in the Huab Basin, NW Namibia: understanding the onset of flood volcanism. *J. Geodyn.,* 28, 393-418.

Jerram, D.A., Mountney, N.P., Howell, J.A. and **Stollhofen, H.** (2000a) The fossilised desert; recent developments in our understanding of the Lower Cretaceous deposits in the Huab Basin, NW Namibia. In: *Henno Martin commemorative volume* (Ed. R.M. Miller), *Com. Geol. Surv. S. W. Africa/Namibia*, 12, 269-278.

Jerram, D.A., Mountney, N.P., Howell, J.A., Long, D. and **Stollhofen, H.** (2000b) Death of a sand sea: an active aeolian erg systematically buried by the Etendeka flood basalts of NW Namibia. *J. Geol. Soc. London,* 157, 513-516.

Jol, H.M., Bristow, C.S., Smith, D.G., Junck, M.B. and **Putnam, P.** (2003) Stratigraphic imaging of the Navajo Sandstone using ground-penetrating radar. *Lead. Edge*., 22, 801-920.

Jones, L.S. and **Blakey, R.C.** (1997) Eolian-fluvial interactions in the Page Sandstone (Middle Jurassic) in south-central Utah, USA – a case study of erg-margin process. *Sed. Geol.*, 109, 181–198.

Jones, F.H., dos Santos Scherer, C.M.S. and **Kuchle, J.** (2015) Facies architecture and stratigraphic evolution of aeolain dune and interdune deposits, Permian Caldeirao Member (Santa Brigida Formation), *Brazil. Sed. Geol*., 337, 133-150.

Jordan, O.D. and **Mountney, N.P.** (2010) Styles of interaction between aeolian, fluvial and shallow marine environments in the Pennsylvanian to Permian lower Cutler beds, south-east Utah, USA. *Sedimentology*, 57, 1357-1385.

Kellogg, E.A. (2000) The grasses: a case study in macroevolution. *Annu Rev Ecol Syst.*, 31, 217–238.

Kocurek, G. (1988) First-order and super bounding surfaces in eolian sequences – Bounding surfaces revisited. *Sed. Geol.*, 56, 193-206.

Kocurek, G. (1991) Interpretation of ancient eolian sand dunes. *Annu. Rev. Earth Planet. Sci.,* 19, 43-75.

Kocurek G. (1999) The aeolian rock record (Yes, Virginia, it exists but it really is rather special to create one). In: A.S. Goudie, I. Livingstone and S. Stokes (Eds.), *Aeolian Environments Sediments and Landforms*, pp. 239-259, John Wiley and Sons Ltd, Chichester.

Kocurek, G. and **Day, M.** (2018) What is preserved in the aeolian rock record? A Jurassic Entrada Sandstone case study at the Utah-Arizona border. *Sedimentology*, 65, 1301-1321.

Kocurek, G. and **Dott, R.H.** (1981) Distinctions and uses of stratification types in the interpretation of eolian sand. *J. Sed. Petrol.,* 51, 579-595.

Kocurek, G. and **Ewing, R.C.** (2005) Aeolian dune field self-organization - implications for the formation of simple versus complex dune field patterns. *Geomorphology*, 72, 94-105.

Kocurek, G. and **Fielder, G.** (1982) Adhesion structures. *J. Sed. Petrol.*, **52,** 1229-1241.

Kocurek, G. and **Havholm, K.G.** (1993) Eolian sequence stratigraphy-a conceptual framework. In: *Siliciclastic Sequence Stratigraphy* (Eds P. Eimer and H. Posamentier), *Am. Assoc. Petrol. Geol. Mem.*, 58, 393–409.

Kocurek, G. and **Lancaster, N.** (1999) Aeolian system sediment state: theory and Mojave Desert Kelso dune field example. *Sedimentology,* 46, 505-515.

Kocurek, G., Carr, M., Ewing, R., Havholm, K.G., Nagar, Y.C. and **Singhvi, A.K.** (2007) White Sands Dune Field, New Mexico: age, dune dynamics, and recent accumulations. *Sed. Geol.*, 197, 313-331.

Kocurek, G., Knight, J. and **Havholm, K.** (1992) Outcrop and semi-regional three-dimensional architecture and reconstruction of a portion of the eolian Page Sandstone (Jurassic). In: *The Three-Dimensional Facies Architecture of Terrigenous Clastic Sediments and its Implications for Hydrocarbon Discovery and Recovery* (Eds A.D. Miall and N. Tyler), *SEPM Spec. Publ.* 3, 25-43.

Kocurek, G., Lancaster, N., Carr, M. and **Frank, A.** (1999) Tertiary Tsondab Sandstone Formation: preliminary bedform reconstruction and comparison to modern Namib Sand Sea dunes. *J. Af. Ear. Sci.*, 29, 629-642.

Kocurek, G., Westerman, R., Hern, C., Tatum, D., Rajapara, H.M. and **Singhvi, A.K.** (2020) Aeolian dune accommodation space for Holocene Wadi Channel Avulsion Strata, Wahiba Dune Field, Oman. *Sed. Geol. 399,* 105612.

Koster, E.A. and **Dijkmans, J.W.A.** (1988) Niveo-aeolian deposits and denivation forms, with special reference to the great Kobuk Sand Dunes, Northwestern Alaska. *Ear. Surf. Proc. Landf.,* 13, 153-170.

Krapovickas, V. (2012). Deposits of the Santa Cruz Formation (late early Miocene): paleohydrologic and paleoclimatic significance. In: *Early Miocene paleobiology in Patagonia: High-latitude paleocommunities of the Santa Cruz Formation* (Eds S. F. Vizcaíno, R. F. Kay and M. S. Bargo), pp. 91–103, Cambridge, Cambridge University Press.

Krystinik, L. F. (1990) Development geology in eolian reservoirs. In: *Modern and ancient eolian deposits: Petroleum Exploration and Production, Rocky Mountain section* (Eds S. G. Fryberger, L. F. Krystinik, and C. J. Schenk), *SEPM*, Denver, Colorado, p. 1-12.

Lallier, F., Caumon, G. Borgomano, J., Viseur, S., Fournier, F., Antoine, C. and **Gentilhomme, T.** (2012) Relevance of the stochastic stratigraphic well correlation approach for the study of complex carbonate settings: application to the Malampaya buildup (Offshore Palawan, Philippines). In: *Advances in Carbonate Exploration and Reservoir Analysis* (Eds J. Garland, J.E. Neilsen, S.E. Laubach and K.J. Whidden), *Geol. Soc. Lon. Spec. Pub.*, 370, 265-275.

Lancaster, N. (2009) Dune morphology and dynamics. In: *Geomorphology of Desert Environments* (Eds A.J. Parsons and A.D. Abrahams), 557-596, Springer.

Lancaster, N. and **Teller, J.T.** (1988) Interdune deposits of Namib Sand Sea, *Sed. Geol.*, 55, 91-107.

Langford, R.P. (1989) Fluvial-aeolian interactions: part 1, modern systems, *Sedimentology,* 36, 1023-1035.

Langford, R. and **Chan, M.A**. (1988) Flood surfaces and deflation surfaces within the Cutler Formation and Cedar Mesa Sandstone (Permian), southeastern Utah. *Geol. Soc. Am. Bul.*, 100, 1541-1549.

Langford, R.P. and **Chan, M.A.** (1989) Fluvial–aeolian interactions: part II, ancient systems. *Sedimentology*, 36, 1037–1051.

Langford, R.P., Pearson, K.M., Duncan, K.A., Tatum, D.M., Adams, L. and **Depret, P.A.** (2008) Eolian topography as a control on deposition incorporating lessons from modern dune seas: Permian Cedar Mesa Sandstone, SE Utah, U.S.A. J. Sed. Res., 78, 410-422.

Leleu, S. and **Hartley, A.J.** (2018) Constraints on synrift intrabasinal horst development from alluvial fan and aeolian deposits (Triassic, Fundy Basin, Nova Scotia). In: *Geology and Geomorphology of Alluvial and Fluvial Fans: Terrestrial and*

Planetary Perspectives (Eds D. Ventra, L. E. Clarke), *Geol. Soc. London. Spec. Pub*. 440, 79-101.

Liesa, C.L., Rodríguez-López, J.P., Ezquerro, L., Alfaro, P., Rodriguez-Pascua, M.A., Lafuente, P., Arlegui, L. and **Simon J.L.** (2016) Facies control on seismites in an alluvial-aeolian system: The Pliocene dunefield of the Teruel half-graben basin (eastern Spain). *Sed. Geol*., 344, 237-252.

Lindquist, S. J. (1983) Nugget Formation reservoir characteristics affecting production in the overthrust belt of southwestern Wyoming. *J. Pet. Tech*., 35, 1355–1365.

Long, D.G.F. (2006) Architecture of pre-vegetation sandy-braided perennial and Ephemeral River deposits in the Paleoproterozoic Athabasca Group, northern Saskatchewan, Canada as indicators of Precambrian fluvial style. *Sed. Geol.,* 190, 71-95.

Long, J.T and **Sharp, R.P.** (1964) Barchan dune movement in Imperial Valley, California. *Geol. Soc. Am. Bull*., 75, 149-156.

Loope, D.B. (1984) Eolian origin of Upper Palaeozoic sandstones, southeastern Utah. *J Sed. Petrol.,* 54, 563-580.

Loope, D.B. (1985) Episodic deposition and preservation of eolian sands: A late Paleozoic example from southeastern Utah. *Geology*, 13, 73-76.

Loope, D.B. (1988) Rhizoliths in ancient eolianites. *Sed. Geol.*, 56, 301-314.

Loope, D.B. and **Rowe C.M.** (2003) Long-lived pluvial episodes during deposition of the Navajo Sandstone. *J. Geol.*, 111, 223-232.

Loope, D.B., Swinehart, J.B. and **Mason, J.P.** (1995) Dune-dammed paleovalleys of the Nebraska Sand Hills- intrinsic versus climatic controls on the accumulation of lake and marsh sediments, *Geol. Soc. Am. Bull.*, 107, 396-406.

McCaleb, J. A. (1979) The role of the geologist in exploitation: Vail Colorado: AAPG Reservoir Fundamentals School.

McKee, E.D. (1966) Structures of dunes at White Sands National Monument, New Mexico (and a comparison with structures of dunes from other selected areas). *Sedimentology*, 7, 1-69.

McKee, E.D. (1979) A study of global sand seas. Geological Society Professional Paper, 1052, USGS Numbered Series, pp. 429, Washington D.C.

McKee, E.D. and **Moiola, R.J.** (1975) Geometry and Growth of the White Sands Dune Field, New Mexico. *J. Res. USGS*, 3, 59-66.

McKenna Neumann, C. (1990) Observations of winter aeolian transport and niveo-aeolian deposition at crater lake, pangnirtung pass, N.W.T., Canada, *Perm. Peri. Proc.,* 1, 235-247.

Meadows, N.S. and **Beach, A.** (1993) Structural and climatic controls on facies distribution in a mixed fluvial and aeolian reservoir: the Triassic Sherwood Sandstone in the Irish Sea. *Geol. Soc. Spec. Pub*., 73, 247-264.

Medici, G., West, L.J. and **Mountney, N.P.** (2016) Characterizing flow pathways in a sandstone aquifer: tectonic vs sedimentary heterogeneities. *J. Contaminant Hydrology*, 194, 36-58.

Medici, G., West, L.J. and **Mountney, N.P.** (2019a) Flow heterogeneities and permeability development in the Triassic UK Sherwood Sandstone Group; insights for reservoir quality. *Geol. J.*, 54, 1361-1378.

Medici, G., West, L.J., Mountney, N.P. and **Welch, M.** (2019b) Review: permeability development in the Triassic Sherwood Sandstone Group (UK), insights for management of fluvio-aeolian aquifers worldwide. *Hydrogeology J.*, 27, 2835-2855.

Melton M.A. (1965) The geomorphic and paleoclimatic significance of alluvial deposits in southern Arizona. *J. Geol.*, 73, 1–38.

Metz, J.M., Grotzinger, J.P., Rubin, D.M., Lewis, K.W., Squyres, S.W. and **Bell, J.F.** (2009) Sulfate-rich eolian and wet interdune deposits, Erebus crater, Meridiani Planum, Mars. *J. Sed. Res.*, 79, 247–264.

Mountney, N.P. (2006a) Periodic accumulation and destruction of aeolian erg sequences in the Permian Cedar Mesa Sandstone, White Canyon, southern Utah. Sedimentology, 53, 789-823.

Mountney, N.P. (2006b) Eolian Facies Models. In: *Facies Models Revisited* (Eds H. Posamentier and R.G. Walker), *SEPM Mem.*, 84, 19-83.

Mountney, N.P. (2012) A stratigraphic model to account for complexity in aeolian dune and interdune successions. *Sedimentology*, 59, 964-989.

Mountney, N.P. and **Howell, J.** (2000) Aeolian architecture, bedform climbing and preservation space in the Cretaceous Etjo Formation, NW Nambia. *Sedimentology*, 47, 825-849.

Mountney, N.P. and **Thompson, D.B.** (2002) Stratigraphic evolution and preservation of aeolian dune and damp/ wet interdune strata: an example from the Triassic Helsby Sandstone Formation, Cheshire Basin, UK. *Sedimentology,* 49, 805-833.

Mountney, N.P. and **Jagger, A.** (2004) Stratigraphic evolution of an aeolian erg margin system: the Permian Cedar Mesa Sandstone, SE Utah, USA. *Sedimentology*, 51, 713-743.

Mountney, N.P. and **Russell, A.J.** (2004) Sedimentology of aeolian sandsheet deposits in the Askja region of northeast Iceland. *Sed. Geol.*, 166, 223-244.

Mountney, N.P. and **Russell, A.J.** (2006) Coastal aeolian dune-field development and response to periodic fluvial inundation, Sólheimasandur, southern Iceland. *Sed. Geol.*, 192, 167-181.

Mountney, N.P., Howell, J.A., Flint, S.S. and **Jerram, D.A.** (1999a) Relating eolian bounding-surface geometries to the bed forms that generated them: Etjo Formation, Cretaceous, Namibia. *Geology,* 27, 159-162.

Mountney, N.P., Howell, J.A., Flint, S.S. and **Jerram, D.A.** (1999b) Climate, sediment supply and tectonics as controls on the deposition and preservation of the aeolian-fluvial Etjo Sandstone Formation, Namibia. *J. Geol. Soc. Lond.,* 156, 771-779.

Nanson, G.C. and **Price, C.D.M.** (1995) Aeolian and fluvial evidence of changing climate and wind patterns during the past 100 ka in the western Simpson Desert, Australia. *Palaeogeog., Palaeoclim., Palaeoecol.*, 113, 87-102.

Nagtegaal, P.J.C. (1979) Relationship of facies and reservoir quality in Rotliegends desert sandstones, southern North Sea region. *J. Pet. Geol.*, 2, 145–158.

Nielson J. and **Kocurek G.** (1986) Climbing zibars of the Algodones. *Sed. Geol.,* 48, 1-15.

Newell, A.J. (2001) Bounding surfaces in a mixed aeolian-fluvial system (Rotliegend, Wessex Basin, SW UK). *Mar. Pet. Geol.*, 18, 339-347.

Nickling, W.G., McKenna Neuman, C. and **Lancaster, N.** (2002) Grainfall processes in the lee of transverse dunes, Silver Peak, Nevada. *Sedimentology*, 49, 191–209.

North, C. P. and **Prosser, D.J.** (1993) Characterization of fluvial and eolian reservoirs: Problems and approaches. In: *Characterization of fluvial and eolian reservoirs* (Eds C. P. North and D. J. Prosser), *Geol. Soc. Spec. Publ.*, 73, p. 1–6.

Olsen, H., Due, P.H. and Clemmensen, L.B. (1989) Morphology and genesis of asymmetric adhesion warts—a new adhesion surface structure. *Sed. Geol.,* 61, 277-285.

Parrish, J.T. and **Peterson, F.** (1988) Wind directions predicted from global circulation models and wind directions determined from Eolian sandstones of the western United States – A comparison. *Sed. Geol.*, 56, 261-282.

Pickup, G.E. and **Hern, C.Y.** (2002) The development of appropriate upscaling procedures. *Trans. Por. Med.*, *46*, 119-138.

Pierce, C. S., Howell, J., Rieke, H. and **Healy, D.** (2016). Geomodeling of aeolian reservoir analogues: A virtual-outcrop based study of the Jurassic page sandstone formation. In: *2nd Conference on Forward Modelling of Sedimentary Systems: From*

Desert to Deep Marine Depositional Systems, European Association of Geoscientists and Engineers, EAGE, p. 67-71.

Pike, J.D. and **Sweet, D.E.** (2018) Environmental drivers of cyclicity recorded in lower Permian eolian strata, Manitou Springs, western United States. *Palaeogeog., Palaeoclim., Palaeoecol.*, 499, 1-12.

Prosser, D. J. and **Maskall, R** (1993) Permeability variation within eolian sandstone: A case study using core cut sub-parallel to slipface bedding, the Auk field, central North Sea, UK: Characterization of fluvial and eolian reservoirs. *Geol. Soc. Spec. Pub.*, 73, 377–397.

Purser, B.H. and **Evans, G.** (1973) Regional sedimentation along the Trucial Coast, Persian Gulf. In: *The Persian Gulf* (Ed. B.H. Purser), p.211-231, Berlin, Springer.

Pye, K. and **Tsoar, H.** (1990) Aeolian sand and sand dune, p. 396, Unwin Hyman Limited, London.

Rainbird, R.H. (1992) Anatomy of a large-scale braid-plain quartzarenite from the Neoproterozoic Shaler Group, Victoria Island, Northwest Territories, Canada. *Can. J. Ear. Sci.*, 29, 2537-2550.

Reis, A.D.d., Scherer, C.M.S., Amarante, F.B., Rossetti, M.M.M., Kifumbi, C., Souza, E.G., Formolo Ferronatto, J.P and **Owen, A.** (2020) Sedimentology of the proximal portion of a large-scale, Upper Jurassic fluvial-aeolian system in Paraná Basin, southwestern Gondwana. *J. S. Am. Ear. Sci.,* 95, 102248.

Ridgley, J.L. (1977) Stratigraphy and depositional environments of Jurassic-Cretaceous sedimentary rocks in the southwest part of the Chama Basin, New Mexico. *New Mexico Geological Society, Guidebook,* 28, 153-158.

Rodríguez-López, J.P. and **Wu, C.** (2020) Recurrent deformations of aeolian desert dunes in the cretaceous of the South China Block: Trigger mechanisms variability and implications for aeolian reservoirs. *Mar. Pet. Geol.,* 119, 104483.

Rodríguez-López, J.P., Meléndez, N., de Boer, P.L. and **Soria, A.R.** (2012) Controls on marine-erg margin cycle variability: aeolian-marine interaction in the Mid-Cretaceous Iberian Desert System, Spain. *Sedimentology*, 59, 466-501.

Rodríguez-López, J.P., Clemmensen, L.B., Lancaster, N., Mountney, N.P and **Veiga, G.D.** (2014) Archean to Recent aeolian sand systems and their sedimentary record: Current understanding and future prospects. *Sedimentology,* 61, 1487–1534.

Ross, G.M. (1981) Bedforms, facies association, and tectono-stratigraphic setting of Proterozoic eolianites, Hornby Bay Group, Northwest Territories, Canada. *Am. Assoc. Petrol. Geol. Bull.*, 65, 981-982.

Rubin, D.M. (1987) Cross-bedding, bedforms and palaeocurrents. *SEPM Concepts Sedimentol. Paleontol.,* **1,** pp. 187.

Rubin, D.M. and **Carter, C.L.** (2006) *Bedforms and Cross-Bedding in Animation*. SEPM, Atlas 2, DVD.

Rubin, D.M. and **Hunter, R.E.** (1982) Migration directions of primary and superimposed dunes inferred from compound crossbedding in the Navajo Sandstone. In: *11th International Congress on Sedimentology, Hamilton, Ontario, August 1982* (Eds J.O. Nriagu and R. Troost), *Int. Assoc. Sedimentol.*, pp. 69-70.

Rubin, D.M. and **Hunter, R.E.** (1985) Why deposits of longitudinal dunes are rarely recognized in the geologic record. *Sedimentology,* **32,** 147-157.

Scherer, C.M.S. (2000) Eolian dunes of the Botucatu Formation (Cretaceous) in southernmost Brazil: morphology and origin. *Sed. Geol.*, 137, 63-84.

Scherer, C.M.S. (2002) Preservation of aeolian genetic units by lava flows in the Lower Cretaceous of the Paraná Basin, southern Brazil. *Sedimentology,* 49, 97-116.

Scherer, C.M.S. and Goldberg, K. (2007) Palaeowind patterns during the latest Jurassic-earliest Cretaceous in Gondwana: Evidence from aeolian cross-strata of the Botucatu Formation, Brazil. *Palaeogeogr. Palaeoclimatol. Palaeoecol.*, 250, 89-100.

Scherer, C.M.A. and **Lavina, L.C.** (2005) Sedimentary cycles and facies architecture of aeolian–fluvial strata of the Upper Jurassic Guara Formation, southern Brazil. *Sedimentology,* 52, 1323-1341.

Scherer, C.M.S. and **Lavina, L.C.** (2006) Stratigraphic evolution of a fluvial–eolian succession: The example of the Upper Jurassic—Lower Cretaceous Guará and Botucatu formations, Paraná Basin, Southernmost Brazil. *Gond. Res.,* 9, 475-484.

Scherer, M.S., Lavina, E.L.C., Dias Filho, D.C., Oliveira, F.M., Bongiolo, D.E. and **Aguiar, E.S.** (2007) Stratigraphy and facies architecture of the fluvial-aeolian-lacustrine Sergi Formation (Upper Jurassic), Reconcavo Basin, Brazil. *Sed. Geol.*, 194, 169-193.

Scherer, C.M.S., Mello, R.G., Ferronatto, J.P.F., Amarante, F.B., Reis, A.D., Souza, E.G., and **Goldberg, K.** (2020) Changes in prevailing surface-palaeowinds of western Gondwana during Early Cretaceous. *Cret. Res.*, 116, 104598

Schokker, J. and **Koster, E.A.** (2004) Sedimentology and facies distribution of Pleistocene cold-climate aeolian and fluvial deposits in the Roer Valley graben (Southeastern Netherlands). *Permafrost and Periglac. Proc.*, 15, 1-20.

Scotti, A. and **Veiga, G.D.** (2019) Sedimentary architecture of an ancient linear megadune (Barremian, Neuquén Basin): Insights into the long-term development and evolution of aeolian linear bedforms. *Sedimentology*, 66, 2191-2213.

Semeniuk V. and **Glassford D.K.** (1988) Significance of aeolian limestone lenses in quartz sand formations: an interdigitation of coastal and continental facies, Perth Basin, southwestern Australia. *Sed. Geol.*, 57, 199-209.

Shaw, R.D., Etheridge, M.A. and **Lambeck, K.** (1991) Development of the Late Proterozoic to Mid-Paleozoic, intracratonic Amadeus Basin in central Australia: A key to understanding tectonic forces in plate interiors. *Tectonics,* 10, 688-721.

Shebi, M. A. (1995) The impact of reservoir heterogeneity on fluid flow in the Tensleep Sandstone of the Bighorn Basin: Resources of southwestern Wyoming, field conference guidebook. *Wyoming Geol. Ass*., p. 343–359.

Shinn, E. (1973) Sedimentary accretion along the leeward SE coast of Qatar Peninsula, Persian Gulf. In: B.H. Purser (Ed.), *The Persian Gulf*, Springer, Berlin, pp. 199-209.

Simplicio, F. and **Basilici, G.** (2015) Unusual thick eolian sand sheet sedimentary succession: Paleoproterozoic Bandeirinha Formation, Minas Gerais. *Braz. J. Geol*., 45, 3-11.

Simpson, E.L., Eriksson, K.A. and **Muller, W.U.** (2012) 3.2 Ga 3.2 Ga eolian deposits from the MoodiesGroup, Barberton Greenstone Belt, South Africa: Implications for the origin of first-cycle quartz sandstones. *Precambrian Res.*, 215, 185-191.

Sorby, H.C. (1859) On the structures produced by the currents present during the deposition of stratified rocks. *The Geol.,* 2, 137-147.

Stanistreet, I.G. and **Stollhofen, H.** (2002) Hoanib River flood deposits of Namib Desert interdunes as analogues for thin permeability barrier mudstone layers in aeolianite reservoirs. *Sedimentology*, 49, 719–736.

Stokes, W.L. (1968) Multiple parallel-truncation bedding planes – a feature of wind deposited sandstone formations. *J. Sed. Petrol.*, 38, 510–515.

Story, C. (1998) Norphlet geology and 3-D geophysics; Fairway Field, Mobile Bay, Alabama. *Lead. Edge*, 17, 243–248.

Strömbäck, A. and **Howell, J.A.** (2002) Predicting distribution of remobilized aeolian facies using sub-surface data: the Weissliegend of the UK Southern North Sea. *Petrol. Geosci.,* 8, 237–249.

Strömbäck, A., Howell, J.A. and **Veiga, G.D.** (2005) The transgression of an erg-sedimentation and reworking/soft-sediment deformation of aeolian facies: the Cretaceous Troncoso Member, Neuquen Basin, Argentina. In: *The Neuquen Basin, Argentina: A Case Study in Sequence Stratigraphy and Basin Dynamics* (Eds G.D. Veiga, G.D. Spaletti, J.A. Howell and E. Schwartz), *Geol. Soc. Spec. Publ.*, 252, 163-183.

Stewart, J.H. (2005) Eolian deposits in the Neoproterozoic Big Bear Group, San Bernardino Mountains, California, USA. *Ear. Sci. Revs.*, 72, 47-62.

Taggart, S., Hampson, G.J. and **Jackson, M.D.** (2010) High-resolution stratigraphic architecture and lithological heterogeneity within marginal aeolian reservoir analogues. *Sedimentology*, 57, 1246-1279

Tatum, D.I. and **Francke, J.** (2012) Constructing hydrocarbon reservoir analogues of aeolian systems using ground penetrating radar. *J. App. Geophys.,* 81, 21-28.

Tatum, D.I. and **Francke, J.** (2012) Radar suitability in aeolian sand dunes – A global review, 14th International Conference on Ground Penetrating Radar (GPR), Shanghai, China.

Taylor, I.E. and **Middleton, G.V.** (1990) Aeolian sandstone in the Copper Harbor Formation, Late Proterozoic, Lake Superior basin. *Can. J. Ear. Sci*., 27, 1339-1347.

Telbisz, T. and **Keszler, O**. (2018) DEM-based morphology of large-scale sand dune patterns in the Grand ERG Oriental (Northern Sahara Desert, Africa). *Arab. J. Geosoc.*, 382.

Thomas, D.S.G. (1988) Analysis of linear dune sediment-from relationships in the Kalahari Dune Desert. *Ear. Surf. Proc. Land*., 13, 545-553.

Thompson, D.B. (1970a) Sedimentation of the Triassic (Scythian) red pebbly sandstones in the Cheshire Basin and its margins. *Geol. J.*, 7, 183-216.

Thompson, D.B. (1970b) The stratigraphy of the so-called Keuper Sandstone Formation (Scythian-?Anisian) in the Permo-Triassic Cheshire Basin. *Q. J. Geol. Soc. Lond.*, 126, 151-181.

Tirsgaard, H. and **Øxnevad, I.E.I.** (1998) Preservation of pre-vegetational mixed fluvio-aeolian deposits in a humid climatic setting: an example from the Middle Proterozoic Eriksfjord Formation, Southwest Greenland. *Sed. Geol.*, 120, 295-317.

Trewin, N.H. (1993) Controls on fluvial deposition in mixed fluvial and aeolian facies within the Tumblagooda Sandstone (Late Silurian) of Western-Australia. *Sed. Geol.,* 85, 387–400.

Veiga, G.D., Spalletti, L.A. and **Flint, S.S.** (2002) Aeolian/fluvial interactions and high-resolution sequence stratigraphy of a non-marine lowstand wedge: the Avile Member of the Agrio Formation (Lower Cretaceous), central Neuquen Basin, Argentina. *Sedimentology*, 49, 1001-1019.

Wasson, R.J and **Hyde, R.** (1983) A test of granulometric control of desert dune geometry. *Ear. Surf. Proc. Land.*, 8, 301-312.

Weber, K. J. (1987) Computation of initial well productivities in eolian sandstone on the basis of a geological model, Leman gas field, UK. In: *Reservoir sedimentology* (Eds R. W. Tillman and K. J. Weber), *SEPM Spec. Pub.*, 40, 333–354.

Vincelette, R.R. and **Chittum, W.E.** (1981) Exploration for oil accumulations in Entrada Sandstone, San Juan Basin, New Mexico. *Bull. Am. Assoc. Pet. Geol.*, 65, 2546-2570.

Voss, R. (2002) Cenozoic stratigraphy of the southern Salar de Antofalla region, northwestern Argentina. *Rev. Geol. Chile*, 29, 167-189.

White, K., Bullard, J., Livingstone, I. and **Moran, L.** (2015) A morphometric comparison of the Namib and southwest Kalahari dunefields using ASTER GDEM data. *Aeolian Res.*, 19, 87-95.

Zavala, C. and **Freije, R.H.** (2001) On the understanding of aeolian sequence stratigraphy: An example from Miocene-Pliocene deposits in Patagonia, Argentina. *Riv. Ital. di Paleont. e Strat.*, 107, 251-264.

Figure Captions

Figure Captions

1. Schematic diagram illustrating subdivisions of major aeolian dune-field (erg) systems, the scales of elements, entities and relationships stored in DASA, and some of its variables. Geomorphic elements represent modern aeolian landforms (i.e. those which are present intact or as remnant forms on the Earth's surface). Architectural elements predominantly represent aeolian and associated non-aeolian deposits preserved in the geological record. DASA stores information on both modern and ancient deposits at a variety of spatial scales. Within a subset

(i.e. a collection of related data), larger scale depositional complex (e.g., a mixed aeolian-fluvial succession) contain individual architectural elements (e.g., a cross-bed dune set), which in turn contain lithofacies (e.g., wind-ripple lamination), which themselves have specific textural and petrophysical properties.

2. Entity-relationship diagram illustrating the tables (entities) of DASA; the relationships between the tables are illustrated by the arrows. The name of each table is shown in capital letters; for each table, primary keys are shown in grey and foreign keys are shown in black. See text for further explanation.

3. Schematic illustration of how subsets, depositional complexes, architectural elements and facies are uniquely indexed in DASA. Each progressively lower-order element is contained (nested) within a higher-order element. A) Subset (original data source); B) depositional complexes are associated with a subset; C) each depositional complex is assigned a unique identifier and recorded in the ‘depositional complex’ table; D) architectural elements are contained within larger-scale depositional complexes; E) each architectural element is assigned a unique identifier and recorded in the ‘architectural element’ table; F) facies are contained within larger-scale architectural elements; G) each facies element is assigned a unique identifier and recorded in the ‘facies element’ table; H) schematic diagram illustrating how transitions between architectural elements are recorded in DASA; I) each architectural element is assigned a unique numerical identifier; J) each element may transition vertically or laterally (lateral transitions are recorded along a direction either parallel or perpendicular to the dominant foreset azimuth) to a different architectural element; each transition is uniquely numbered and the orientation of that transition is recorded; K) the spatial transition between architectural elements may occur across a surface (e.g., an interdune migration

bounding surface); each surface is assigned a unique numerical identifier and various attributes associated with each surface are recorded. The methodology of recording architectural-element transitions and bounding surfaces is shown in parts H-K; an equivalent methodology is also employed for both depositional complexes and facies elements, and their transitions.

4. Schematic diagram illustrating how subsets, depositional complexes, architectural elements and facies elements are recorded in DASA. A) Example of a subset (stratigraphic log); subsets are subdivided into primary and secondary depositional complex types. B) Example of a depositional complex with marine primary type and aeolian secondary type. C) Example of a depositional complex with aeolian primary type and fluvial secondary type. D) Depositional complexes are subdivided into architectural elements of different types. E) Architectural elements are subdivided into facies of different types. F) For each facies, different types of data are recorded, for example on dominant lamination types and on any secondary physical, biogenic or chemical disturbance or alteration.
5. A) Global map illustrating the location of all modern case studies currently contained within DASA; B) bar chart displaying the various data types associated with modern subsets; C) bar chart displaying the latitudinal range of each of the modern case studies within DASA; D) Global map illustrating the location of all ancient case studies currently contained within DASA; E) bar chart displaying the various data types associated with ancient subsets; categories for additional source-data types are already enabled; the classification can be extended further, should new data types be incorporated; F) bar chart displaying the palaeo-latitudinal range of each of the ancient case-studies within DASA. The numbered locations shown in part A and D are outlined in Tables 1 and 2, respectively.

6. A-F) Scatter plots displaying relationships between pairs of geometric parameters of modern (geomorphic) dune elements (A-C), and ancient dune-set elements (D-F), coloured by interpreted dune type. G) Box-and-whisker plots comparing various heights of modern dunes and thicknesses of ancient dune sets, for various interpreted dune types. H) Scatter plot showing the mean height (modern dune) and mean thickness (ancient dune sets) for all dune elements in DASA, coloured by interpreted dune type. The grey crosses for each data point indicate one standard deviation from the mean; the 'n =' refers to the total number of modern and ancient dunes. I) Schematic diagram illustrating the dune types as defined in DASA. Blue arrows indicate significant wind directions relative to bedform orientation.
7. A) Schematic diagram illustrating palaeogeographic configurations of selected times of supercontinent assemblage, denoted as follows: 1 = Proterozoic Supercontinent; 2 = Gondwanaland; 3 = Pangaea; 4 = dispersed continental setting. B-E) Pie charts showing the proportions of dune set, sandsheet and interdune elements for each supercontinental setting. F) Box-and-whisker plot illustrating distributions in dune-set thickness for each supercontinental setting. G-H) Scatter plots displaying relationships between geometric parameters of dune set elements, coloured by supercontinental setting. I) Box-and-whisker plot illustrating distributions of sandsheet thickness for each supercontinental setting. J) Probability density function and K) cumulative density plots showing sandsheet thicknesses within each supercontinental setting. L) Box-and-whisker plot illustrating distributions in interdune thickness for each supercontinental setting. M-P) Pie charts illustrating the proportions of wet, dry and damp interdunes for each

supercontinental setting. Q) Scatter plots displaying interdune thickness vs. palaeolatitude, coloured by supercontinental setting.

8. A) Examples of various facies types recorded within DASA and some of the larger-scale architectural elements in which the various facies occur most commonly; each facies is numbered and corresponds with the presented legend. B-C) Scatter plots between geometric parameters of facies elements, coloured by facies type. D-E) Box-and-whisker plots illustrating distributions in: D) the modal grain size and E) thickness of each facies type.
9. A-C) Idealized block models of: A) adhesion strata, B) interfingered strata and C) wind-ripple strata. D-F) Stacked bar charts illustrating the relative proportion of different architectural-element types in which the above facies are most likely to occur. G-I) Stacked bar charts illustrating the relative frequency of different modal sand grain-size classes of the above facies types. DASA can also record intermediate grain-size classes (e.g., lower-fine, upper-fine etc.), but these are not reported here.
10. A-C) Hypothetical example of how transitions between architectural elements of different types are recorded in DASA. A) Hypothetical vertical log through an aeolian succession; B) vertical section and the transitions (T1 to T8) between the various architectural element types (no particular scale implied); C) description of the architectural element transitions in the hypothetical vertical log. The hypothetical example presented in parts A-C is for illustrative purposes only and does not reflect the real data summarized in parts D-F. D) Heatmap showing vertical transition probabilities between classes of architectural elements for all data currently stored in DASA. The architectural-element types are denoted as follows: 1 = dune set; 2 = sandsheet; 3 = dry interdune; 4 = damp interdune; 5 =

wet interdune; 6 = all non-aeolian deposits. Underlying architectural elements are listed on the vertical axis of the heatmap; overlying architectural elements are listed on the horizontal axis and are additionally denoted with ‘V’ (for “vertical") in parenthesis. E-F) stacked bar charts illustrating the percentage of vertical element transitions from one element type to another; in Part E all transitions to non-aeolian elements are grouped in a single category; in Part F, vertical transitions relating exclusively to the non-aeolian element types are shown in detail.

11. Two examples of sequential surface filtering. A) The percentage of recorded surfaces that are supersurfaces (A1), *and* are Mesozoic in age (A2), *and* are associated with wet surface sedimentary features (A3), *and* are classed as bypass surfaces (A4). B) The percentage of recorded surfaces that are interdunes (B1), *and* are deposited in palaeolatitudes of between 15-30º (B2), *and* have a curved shape (B3), *and* are classed as a ‘damp’ type (B4). The arrows indicate the sequential levels of filtering.

12. A) Schematic diagram illustrating the occurrence of four major aeolian bounding surface types (supersurface, interdune migration, superposition and reactivation), their occurrence within an aeolian system, and their interactions with each other. B-C) Box plots showing distributions of surface lengths along directions that are, respectively, parallel (B) and perpendicular (C) to foreset dip. D-G) Bar charts illustrating the frequency of occurrence of various properties associated with the four surface types; D) the frequency of surfaces classified as bypass or deflation type; E) the frequency of surfaces classified as dry, damp or wet; F) the frequency of surfaces classified as stabilized or unstabilized; G) the frequency of surfaces classified as having a shape that is asymptotic (curved), irregular, planar, scalloped or trough.

13. Example of how DASA can be applied to generate highly specific outputs suitable for the generation of bespoke quantitative facies models. A) Schematic diagram illustrating classes of dune-field location as recorded in DASA. “Margin” refers to lateral dune-field (erg) margins. B) Scatter plot of architectural-element thickness and length, for elements of any type, coloured by dune-field location. C) Stacked bar charts showing the percentages of different architectural-element types across different classes of dune-field location. D) Schematic diagram illustrating the erg centre. E) Scatter plot reporting architectural-element thickness and length for aeolian architectural element types from central-erg settings. Colours indicate aeolian element types; all aeolian element types are defined in Table 4. F) Box-and-whisker plot showing thickness distributions for different aeolian element types from erg-centre settings. G) Schematic diagram illustrating cross-bedded dune sets in central-erg settings. H-I) Probability density functions showing (H) dune-set thickness and (I) dune-set length and width in erg-centre settings. J) Schematic diagram illustrating some of the properties of cross-bedded dune sets recorded in DASA. K) Scatter plot showing dune-set thickness vs. dune-set length, coloured by the shape of the bounding surface that defines the shape of the base of the element, for all cross-bedded dune sets from erg-centre settings. L-O) Pie-charts showing the frequency of occurrence of various properties of cross-bedded dune sets from erg-centre settings, as follows: L) proportion of surfaces described as conformable or truncating; M) proportion of dune sets described as solitary or grouped; N) proportion of various facies within dune sets; O) proportion of various grain-size classes within dune sets.
14. Example of how DASA can be applied to generate highly specific outputs suitable for the generation of bespoke quantitative facies models. A) Schematic diagram

illustrating examples of various primary and secondary depositional types. Box-and-whisker plots showing the thickness distributions of B) primary and C) secondary depositional complexes. D) Schematic diagram showing dune-set, sandsheet and interdune elements within an exclusively aeolian depositional system. E) Scatter plot showing the relationship between the thickness and length of dune-set, sandsheet and interdune elements. F) Probability density function showing the thickness of dune set, sandsheet and interdune architectural elements. G) Schematic diagram illustrating how DASA can be filtered for various spatio-temporal characteristics. H-I) Box-and-whisker plots showing the thickness distributions of interdune architectural elements from (H) different supercontinental settings and (I) basin settings. The Pangaean supercontinental setting is highlighted with a red box; this particular spatio-temporal setting is interrogated further in parts K and L. J) Schematic diagram illustrating the texture and facies of interdune elements. K) Proportion of dry, damp and wet interdune architectural elements in Pangaean supercontinental settings only. L) Proportions of different facies elements within dry, damp, and wet interdune elements in Pangaean supercontinental settings.

Table Captions

1. Case study names, locations and associated references of the modern aeolian systems included in DASA.
2. Case study names, locations and associated references of the ancient aeolian systems included in DASA.

3. Depositional-complex types used in DASA for the classification of overall depositional setting. Each depositional complex can be used as a primary or secondary complex-type descriptor.
4. Examples of DASA sub-environment and architectural-element types for the classification of architectural and geomorphic elements; only the aeolian architectural and geomorphic elements discussed in this article are included here.
5. Examples of DASA facies types for the classification of facies units.

Figure 1

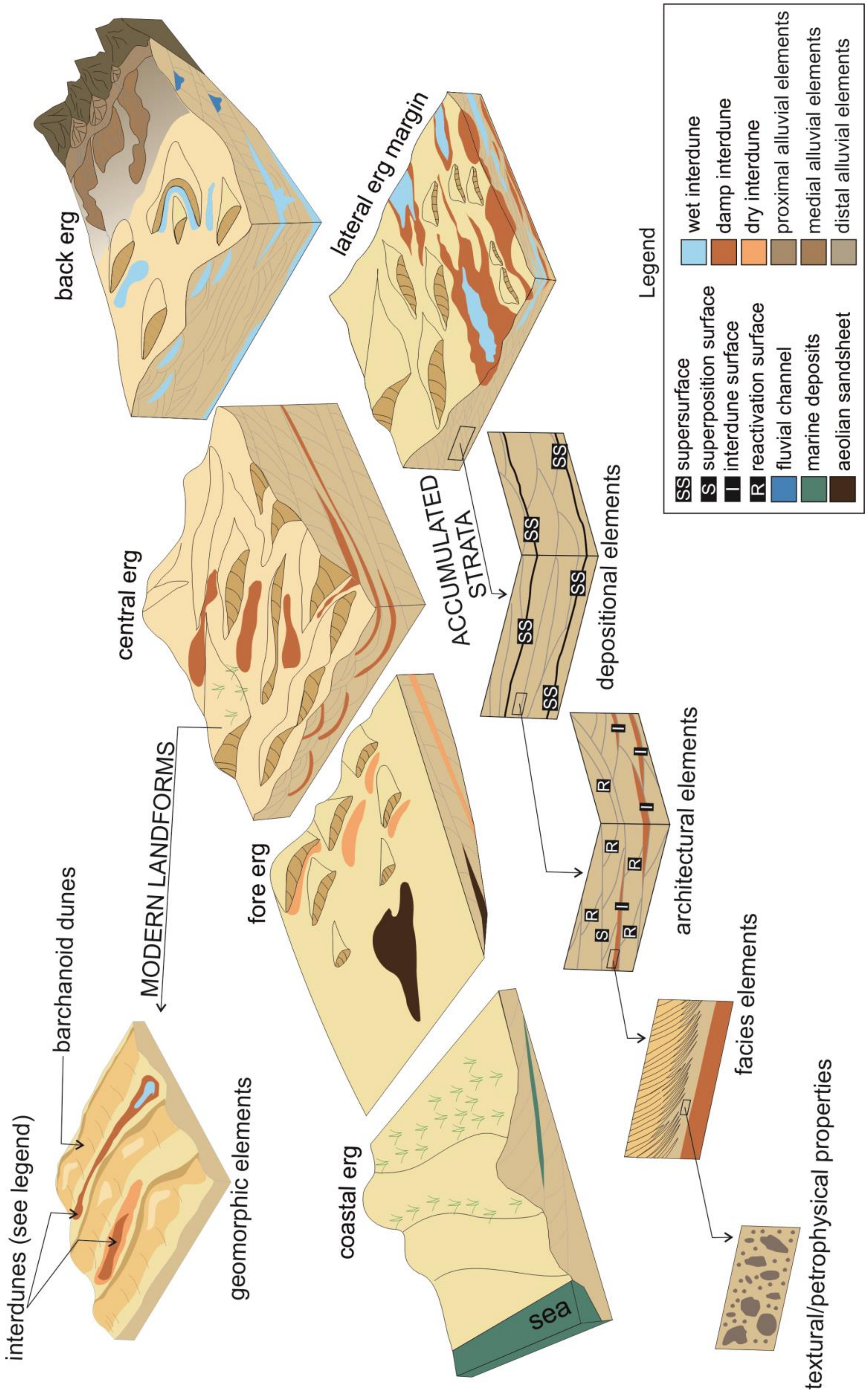
back erg
lateral erg margin
central erg
fore erg
coastal erg
sea
MODERN LANDFORMS
ACCUMULATED STRATA
barchanoid dunes
interdunes (see legend)
geomorphic elements
depositional elements
architectural elements
facies elements
textural/petrophysical properties
SS
S
I
R
Legend
SS supersurface
S superposition surface
I interdune surface
R reactivation surface
fluvial channel
marine deposits
aeolian sandsheet
wet interdune
damp interdune
dry interdune
proximal alluvial elements
medial alluvial elements
distal alluvial elements

Figure 2

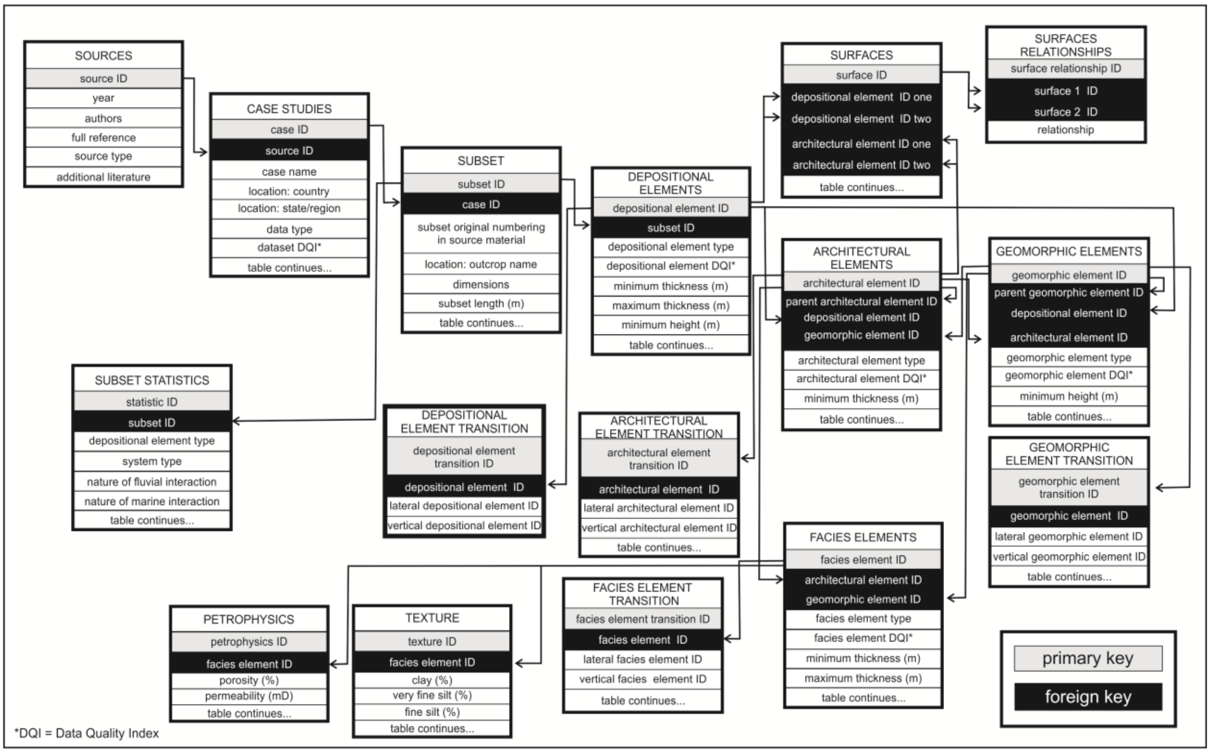

SOURCES
source ID
year
authors
full reference
source type
additional literature
CASE STUDIES
case ID
source ID
case name
location: country
location: state/region
data type
dataset DQI*
table continues...
SUBSET
subset ID
case ID
subset original numbering in source material
location: outcrop name
dimensions
subset length (m)
table continues...
DEPOSITIONAL ELEMENTS
depositional element ID
subset ID
depositional element type
depositional element DQI*
minimum thickness (m)
maximum thickness (m)
minimum height (m)
table continues...
SURFACES
surface ID
depositional element ID one
depositional element ID two
architectural element ID one
architectural element ID two
table continues...
SURFACES RELATIONSHIPS
surface relationship ID
surface 1 ID
surface 2 ID
relationship
ARCHITECTURAL ELEMENTS
architectural element ID
parent architectural element ID
depositional element ID
geomorphic element ID
architectural element type
architectural element DQI*
minimum thickness (m)
table continues...
GEOMORPHIC ELEMENTS
geomorphic element ID
parent geomorphic element ID
depositional element ID
architectural element ID
geomorphic element type
geomorphic element DQI*
minimum height (m)
table continues...
SUBSET STATISTICS
statistic ID
subset ID
depositional element type
system type
nature of fluvial interaction
nature of marine interaction
table continues...
DEPOSITIONAL ELEMENT TRANSITION
depositional element transition ID
depositional element ID
lateral depositional element ID
vertical depositional element ID
ARCHITECTURAL ELEMENT TRANSITION
architectural element transition ID
architectural element ID
lateral architectural element ID
vertical architectural element ID
table continues...
GEOMORPHIC ELEMENT TRANSITION
geomorphic element transition ID
geomorphic element ID
lateral geomorphic element ID
vertical geomorphic element ID
table continues...
FACIES ELEMENTS
facies element ID
architectural element ID
geomorphic element ID
facies element type
facies element DQI*
minimum thickness (m)
maximum thickness (m)
table continues...
FACIES ELEMENT TRANSITION
facies element transition ID
facies element ID
lateral facies element ID
vertical facies element ID
table continues...
PETROPHYSICS
petrophysics ID
facies element ID
porosity (%)
permeability (mD)
table continues...
TEXTURE
texture ID
facies element ID
clay (%)
very fine silt (%)
fine silt (%)
table continues...
primary key
foreign key
*DQI = Data Quality Index

Figure 3

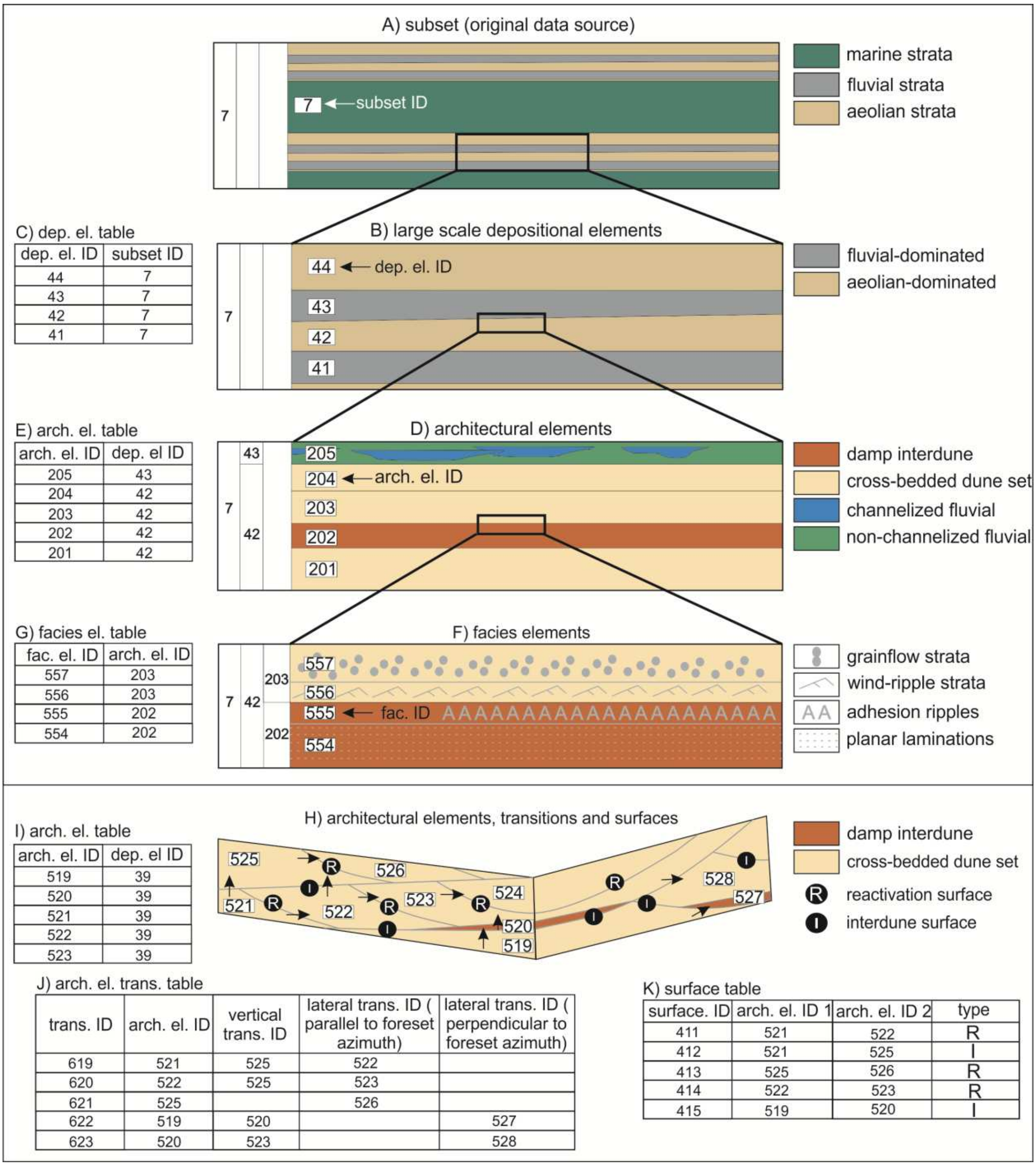

C) dep. el. table

dep. el. ID	subset ID
44	7
43	7
42	7
41	7

E) arch. el. table

arch. el. ID	dep. el ID
205	43
204	42
203	42
202	42
201	42

G) facies el. table

fac. el. ID	arch. el. ID
557	203
556	203
555	202
554	202

I) arch. el. table

arch. el. ID	dep. el ID
519	39
520	39
521	39
522	39
523	39

J) arch. el. trans. table

trans. ID	arch. el. ID	vertical trans. ID	lateral trans. ID (parallel to foreset azimuth)	lateral trans. ID (perpendicular to foreset azimuth)
619	521	525	522	
620	522	525	523	
621	525		526	
622	519	520		527
623	520	523		528

K) surface table

surface. ID	arch. el. ID 1	arch. el. ID 2	type
411	521	522	R
412	521	525	I
413	525	526	R
414	522	523	R
415	519	520	I

Figure 4

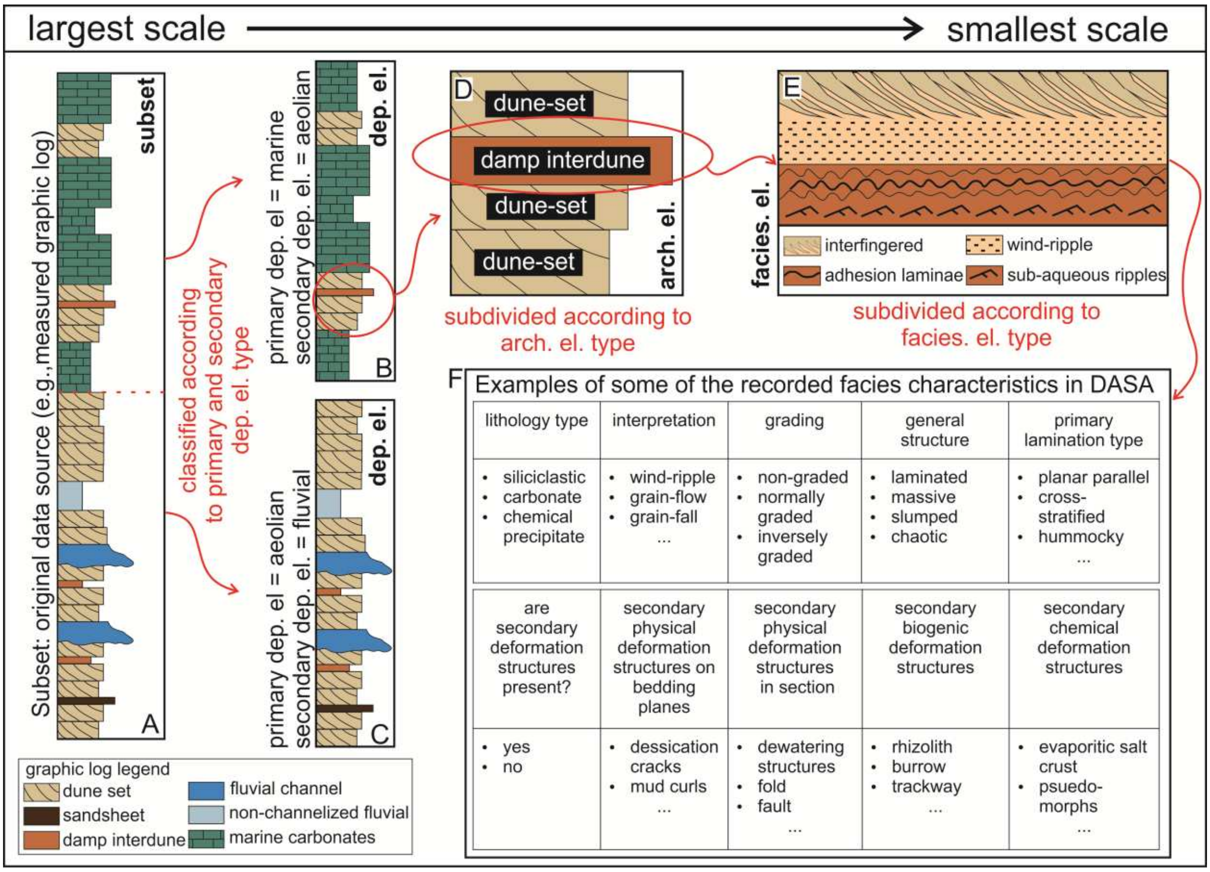

Figure 5

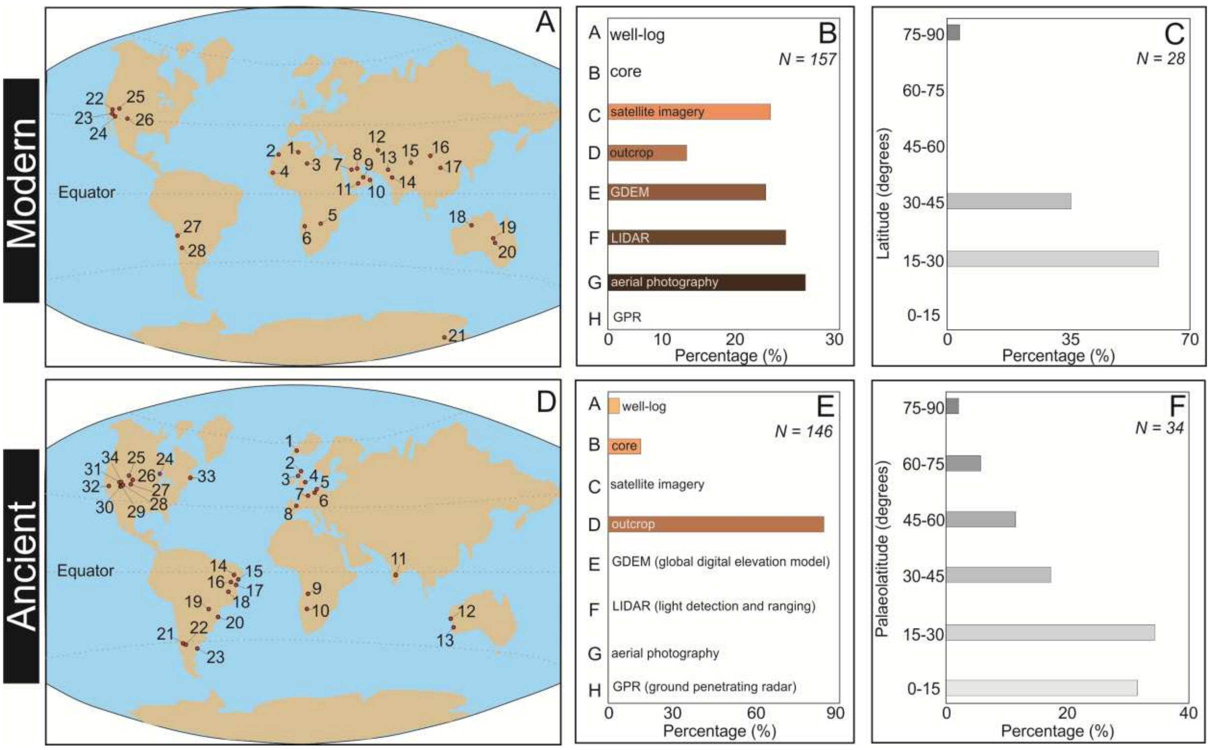

Figure 6

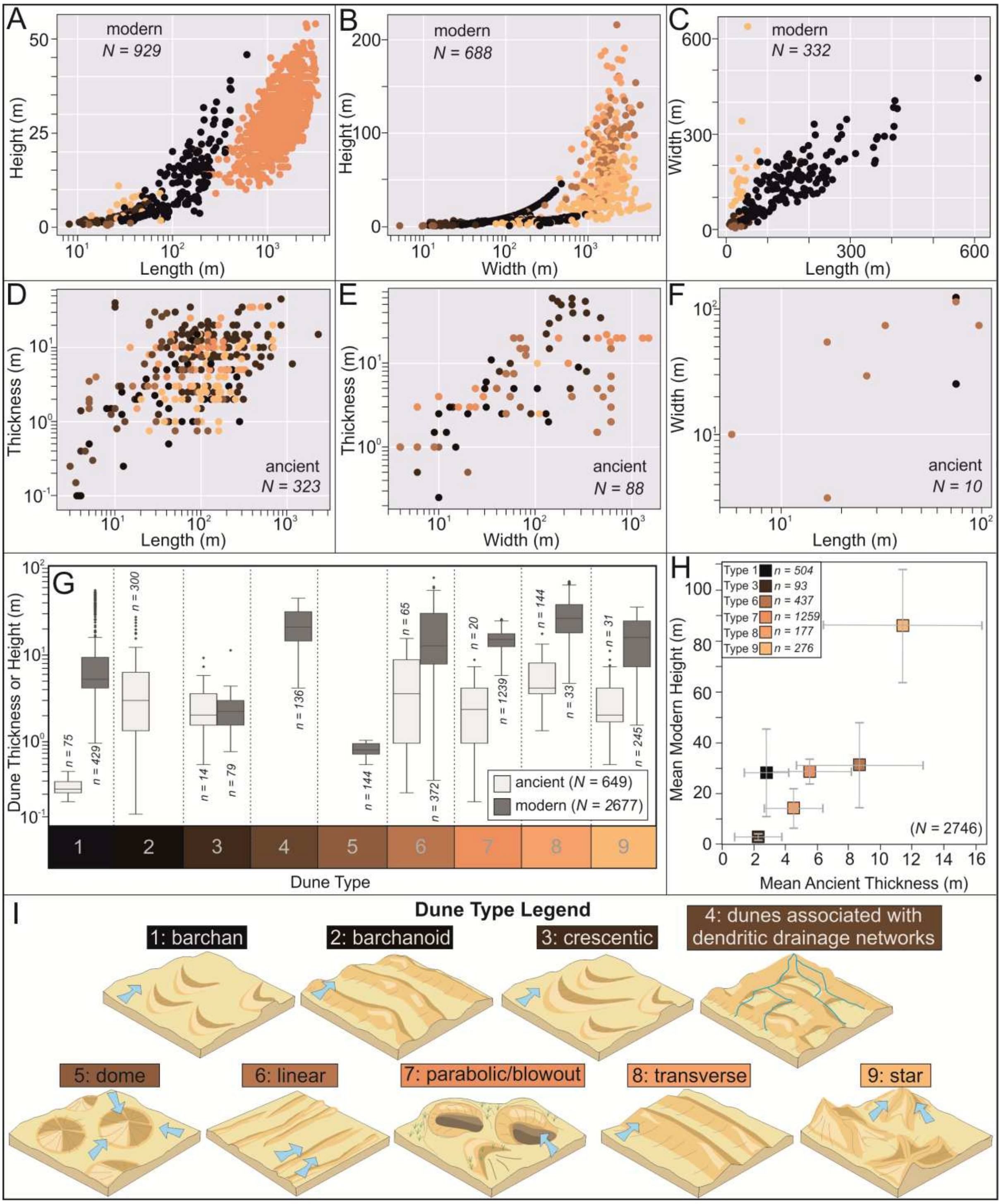
A
modern
N = 929
Height (m)
Length (m)
B
modern
N = 688
Height (m)
Width (m)
C
modern
N = 332
Width (m)
Length (m)
D
ancient
N = 323
Thickness (m)
Length (m)
E
ancient
N = 88
Thickness (m)
Width (m)
F
ancient
N = 10
Width (m)
Length (m)
G
Dune Thickness or Height (m)
ancient (N = 649)
modern (N = 2677)
Dune Type
H
Type 1 n = 504
Type 3 n = 93
Type 6 n = 437
Type 7 n = 1259
Type 8 n = 177
Type 9 n = 276
(N = 2746)
Mean Modern Height (m)
Mean Ancient Thickness (m)
I
Dune Type Legend
1: barchan
2: barchanoid
3: crescentic
4: dunes associated with dendritic drainage networks
5: dome
6: linear
7: parabolic/blowout
8: transverse
9: star

Figure 7

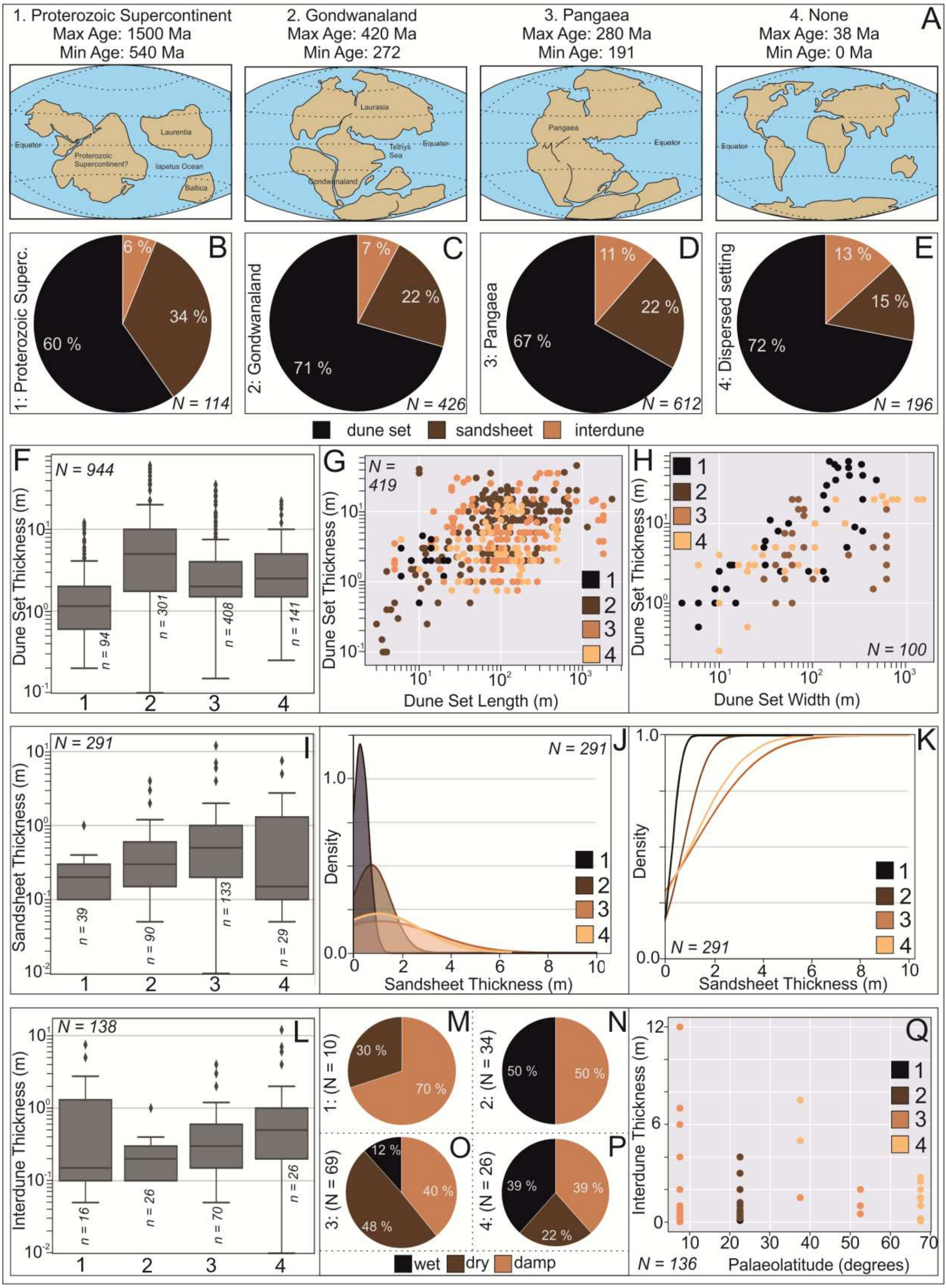

1. Proterozoic Supercontinent
Max Age: 1500 Ma
Min Age: 540 Ma
2. Gondwanaland
Max Age: 420 Ma
Min Age: 272
3. Pangaea
Max Age: 280 Ma
Min Age: 191
4. None
Max Age: 38 Ma
Min Age: 0 Ma
A
Laurentia
Equator
Proterozoic Supercontinent?
Iapetus Ocean
Baltica
Laurasia
Tethys Sea
Gondwanaland
Pangaea
B
1: Proterozoic Superc.
6 %
34 %
60 %
N = 114
C
2: Gondwanaland
7 %
22 %
71 %
N = 426
D
3: Pangaea
11 %
22 %
67 %
N = 612
E
4: Dispersed setting
13 %
15 %
72 %
N = 196
dune set
sandsheet
interdune
F
N = 944
Dune Set Thickness (m)
n = 94
n = 301
n = 408
n = 141
G
N = 419
Dune Set Thickness (m)
Dune Set Length (m)
H
Dune Set Thickness (m)
Dune Set Width (m)
N = 100
I
N = 291
Sandsheet Thickness (m)
n = 39
n = 90
n = 133
n = 29
J
N = 291
Density
Sandsheet Thickness (m)
K
Density
N = 291
Sandsheet Thickness (m)
L
N = 138
Interdune Thickness (m)
n = 16
n = 26
n = 70
n = 26
M
1: (N = 10)
30 %
70 %
N
2: (N = 34)
50 %
50 %
O
3: (N = 69)
12 %
40 %
48 %
P
4: (N = 26)
39 %
39 %
22 %
wet
dry
damp
Q
Interdune Thickness (m)
N = 136
Palaeolatitude (degrees)

Figure 8

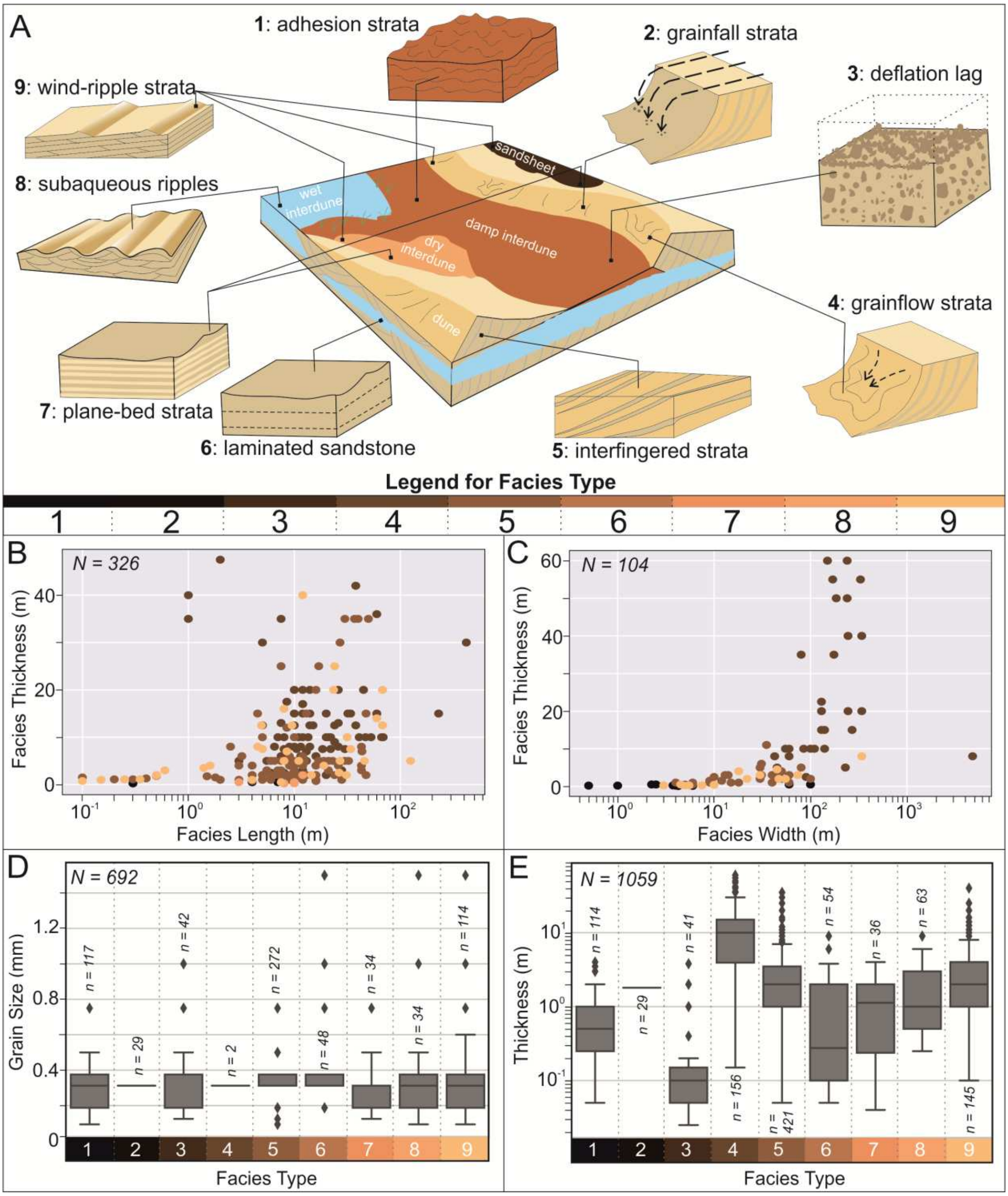
A
1: adhesion strata
2: grainfall strata
3: deflation lag
4: grainflow strata
5: interfingered strata
6: laminated sandstone
7: plane-bed strata
8: subaqueous ripples
9: wind-ripple strata
sandsheet
wet interdune
damp interdune
dry interdune
dune
Legend for Facies Type
1
2
3
4
5
6
7
8
9
B
N = 326
Facies Thickness (m)
Facies Length (m)
C
N = 104
Facies Thickness (m)
Facies Width (m)
D
N = 692
Grain Size (mm)
Facies Type
n = 117
n = 29
n = 42
n = 2
n = 272
n = 48
n = 34
n = 34
n = 114
E
N = 1059
Thickness (m)
Facies Type
n = 114
n = 29
n = 41
n = 156
n = 421
n = 54
n = 36
n = 63
n = 145

Figure 9

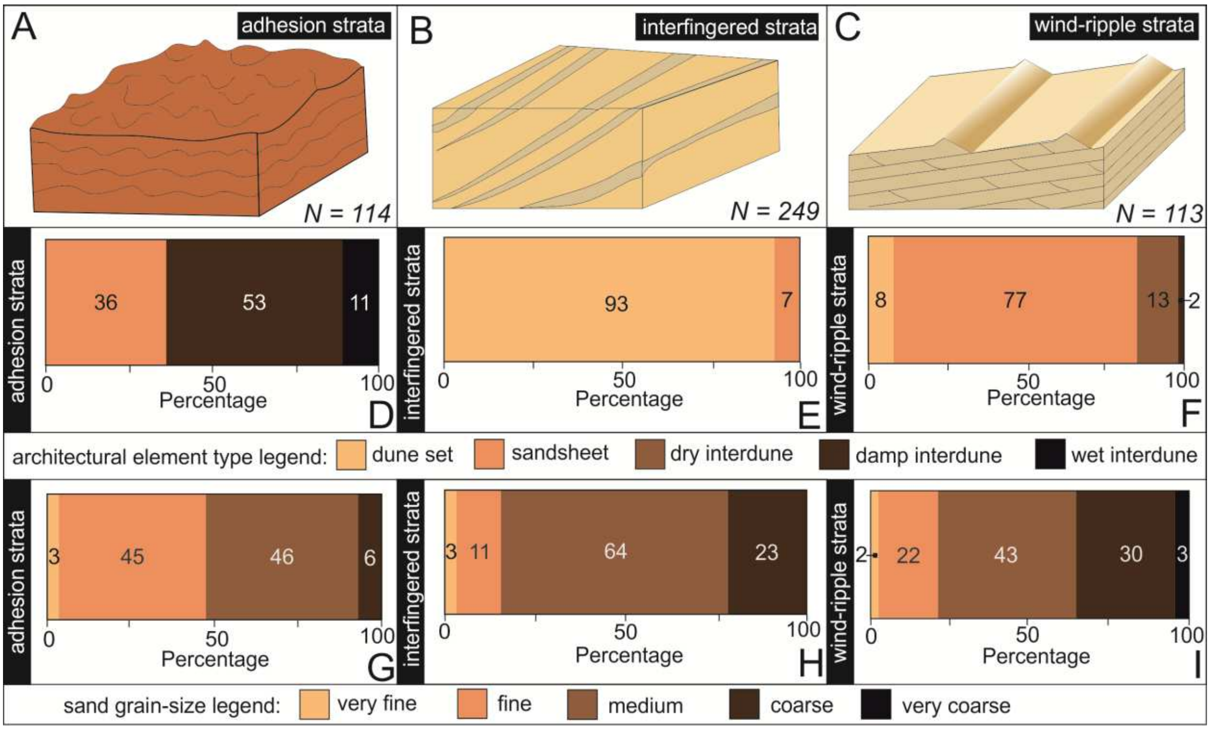
A
adhesion strata
N = 114
B
interfingered strata
N = 249
C
wind-ripple strata
N = 113
adhesion strata
36
53
11
0
50
100
Percentage
D
interfingered strata
93
7
0
50
100
Percentage
E
wind-ripple strata
8
77
13
2
0
50
100
Percentage
F
architectural element type legend:
dune set
sandsheet
dry interdune
damp interdune
wet interdune
adhesion strata
3
45
46
6
0
50
100
Percentage
G
interfingered strata
3
11
64
23
0
50
100
Percentage
H
wind-ripple strata
2
22
43
30
3
0
50
100
Percentage
I
sand grain-size legend:
very fine
fine
medium
coarse
very coarse

Figure 10

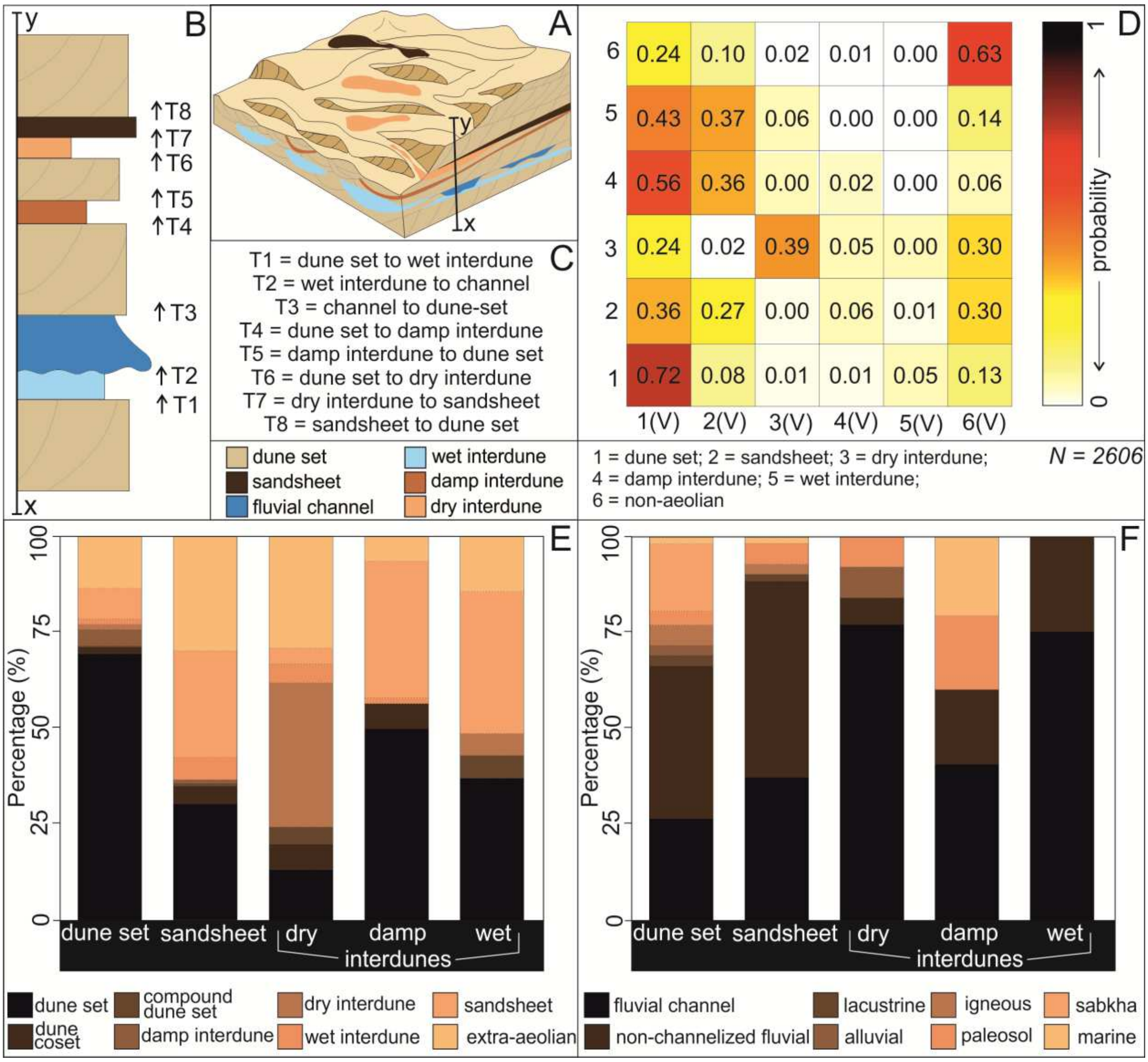
A
B
C
D
E
F
y
x
↑T8
↑T7
↑T6
↑T5
↑T4
↑T3
↑T2
↑T1
T1 = dune set to wet interdune
T2 = wet interdune to channel
T3 = channel to dune-set
T4 = dune set to damp interdune
T5 = damp interdune to dune set
T6 = dune set to dry interdune
T7 = dry interdune to sandsheet
T8 = sandsheet to dune set
dune set
sandsheet
fluvial channel
wet interdune
damp interdune
dry interdune
6 0.24 0.10 0.02 0.01 0.00 0.63
5 0.43 0.37 0.06 0.00 0.00 0.14
4 0.56 0.36 0.00 0.02 0.00 0.06
3 0.24 0.02 0.39 0.05 0.00 0.30
2 0.36 0.27 0.00 0.06 0.01 0.30
1 0.72 0.08 0.01 0.01 0.05 0.13
1(V) 2(V) 3(V) 4(V) 5(V) 6(V)
probability
1
0
1 = dune set; 2 = sandsheet; 3 = dry interdune;
4 = damp interdune; 5 = wet interdune;
6 = non-aeolian
N = 2606
Percentage (%)
0
25
50
75
100
dune set
sandsheet
dry
damp
wet
interdunes
dune set
compound dune set
dry interdune
sandsheet
dune coset
damp interdune
wet interdune
extra-aeolian
fluvial channel
lacustrine
igneous
sabkha
non-channelized fluvial
alluvial
paleosol
marine

Figure 11

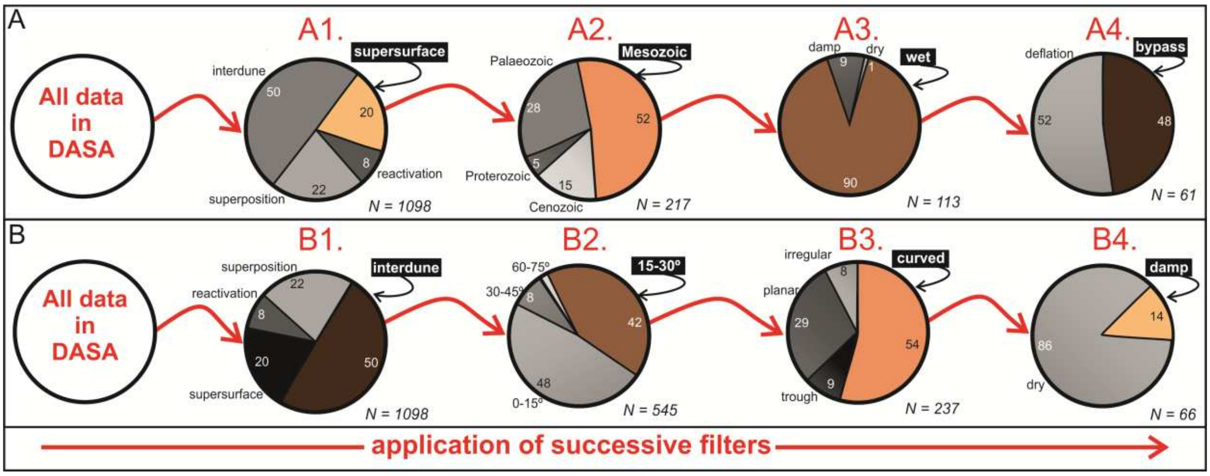

Figure 12

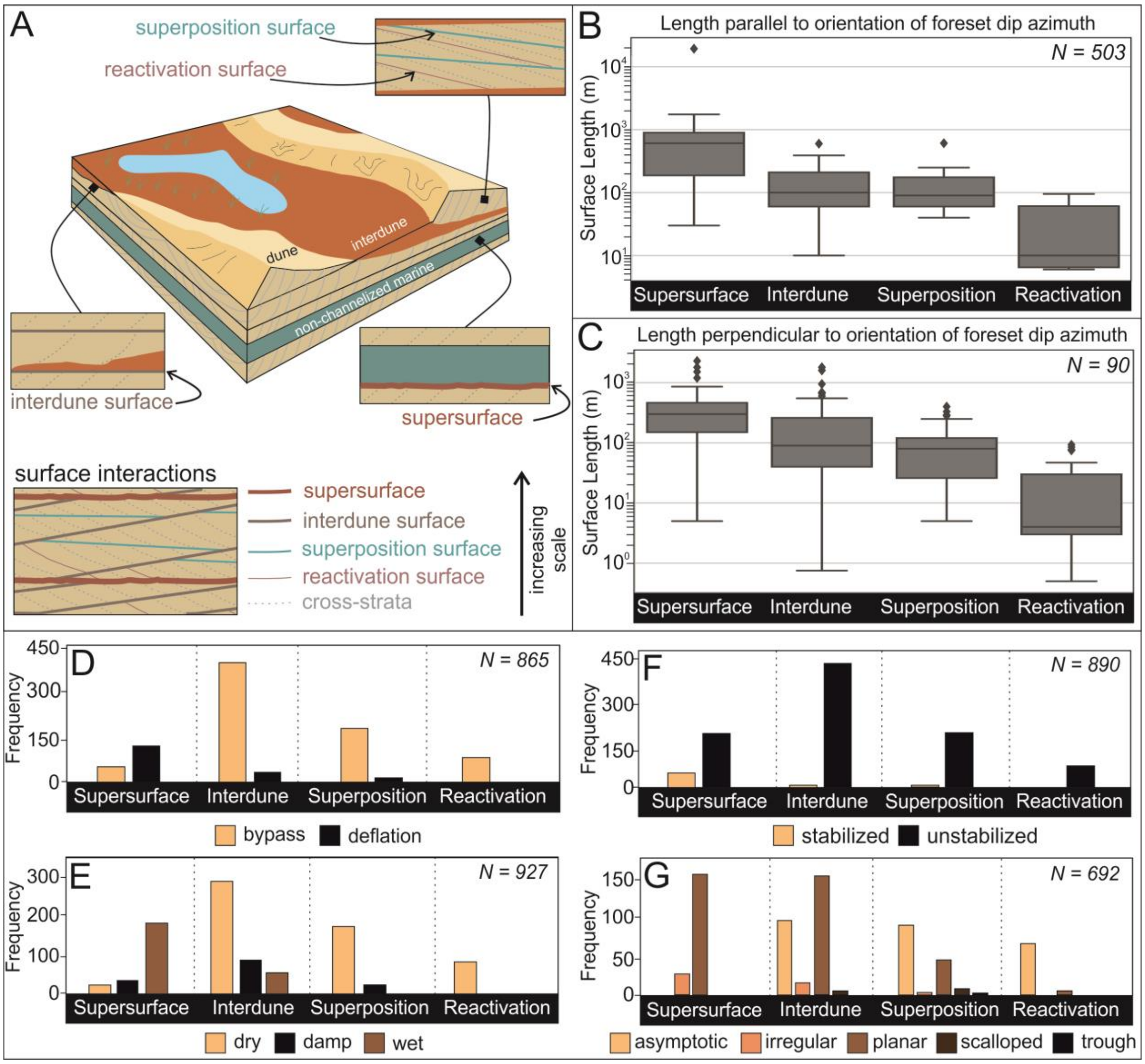

Figure 13

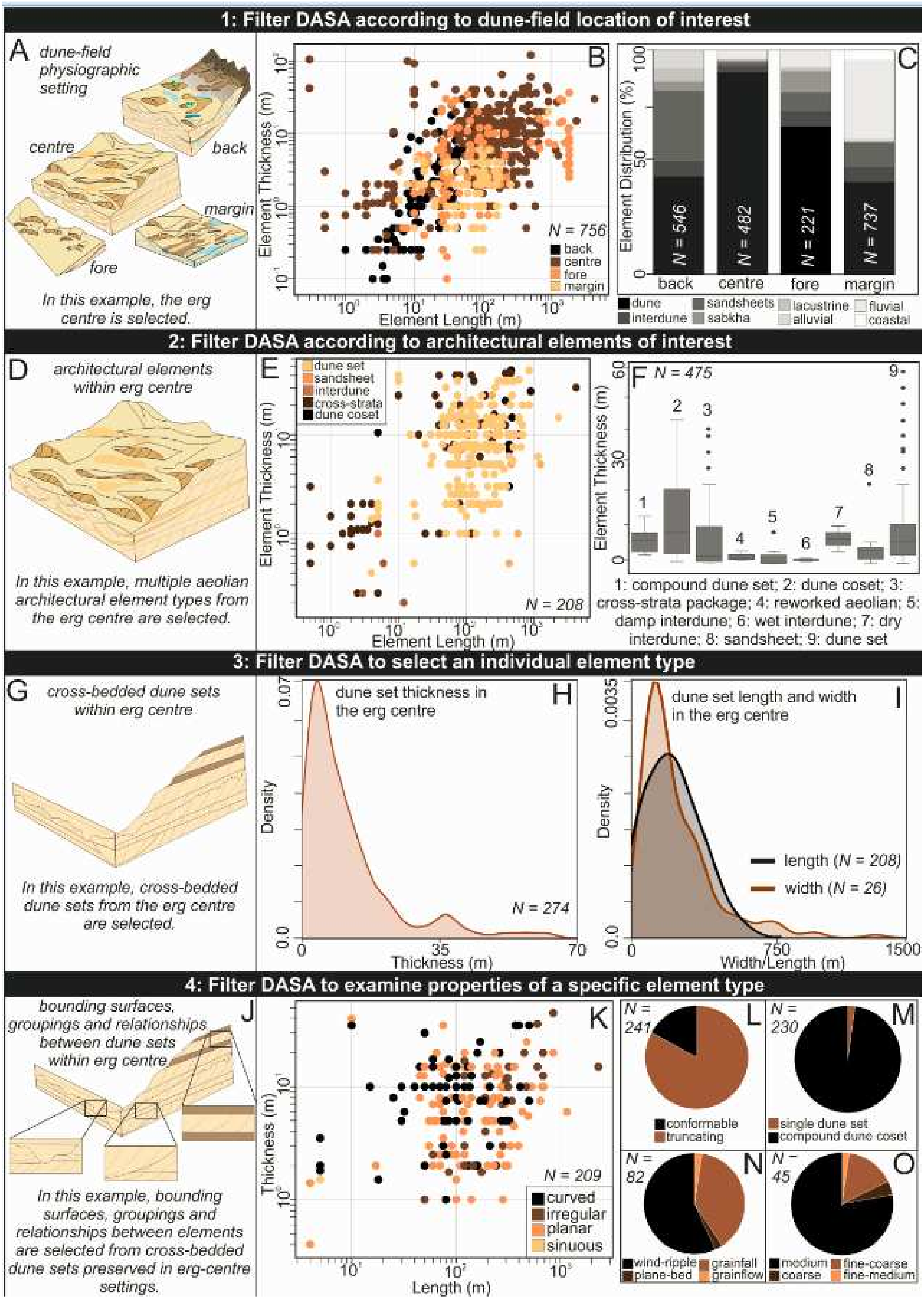

1: Filter DASA according to dune-field location of interest
A
dune-field physiographic setting
centre
back
margin
fore
In this example, the erg centre is selected.
B
Element Thickness (m)
Element Length (m)
N = 756
back
centre
fore
margin
C
Element Distribution (%)
N = 546
N = 482
N = 221
N = 737
back
centre
fore
margin
dune
interdune
sandsheets
sabkha
lacustrine
alluvial
fluvial
coastal
2: Filter DASA according to architectural elements of interest
D
architectural elements within erg centre
In this example, multiple aeolian architectural element types from the erg centre are selected.
E
dune set
sandsheet
interdune
cross-strata
dune coset
Element Thickness (m)
Element Length (m)
N = 208
F
N = 475
Element Thickness (m)
1: compound dune set; 2: dune coset; 3: cross-strata package; 4: reworked aeolian; 5: damp interdune; 6: wet interdune; 7: dry interdune; 8: sandsheet; 9: dune set
3: Filter DASA to select an individual element type
G
cross-bedded dune sets within erg centre
In this example, cross-bedded dune sets from the erg centre are selected.
H
dune set thickness in the erg centre
Density
Thickness (m)
N = 274
I
dune set length and width in the erg centre
Density
length (N = 208)
width (N = 26)
Width/Length (m)
4: Filter DASA to examine properties of a specific element type
J
bounding surfaces, groupings and relationships between dune sets within erg centre
In this example, bounding surfaces, groupings and relationships between elements are selected from cross-bedded dune sets preserved in erg-centre settings.
K
Thickness (m)
Length (m)
N = 209
curved
irregular
planar
sinuous
L
N = 241
conformable
truncating
M
N = 230
single dune set
compound dune coset
N
N = 82
wind-ripple
plane-bed
grainfall
grainflow
O
N = 45
medium
coarse
fine-coarse
fine-medium

Figure 14

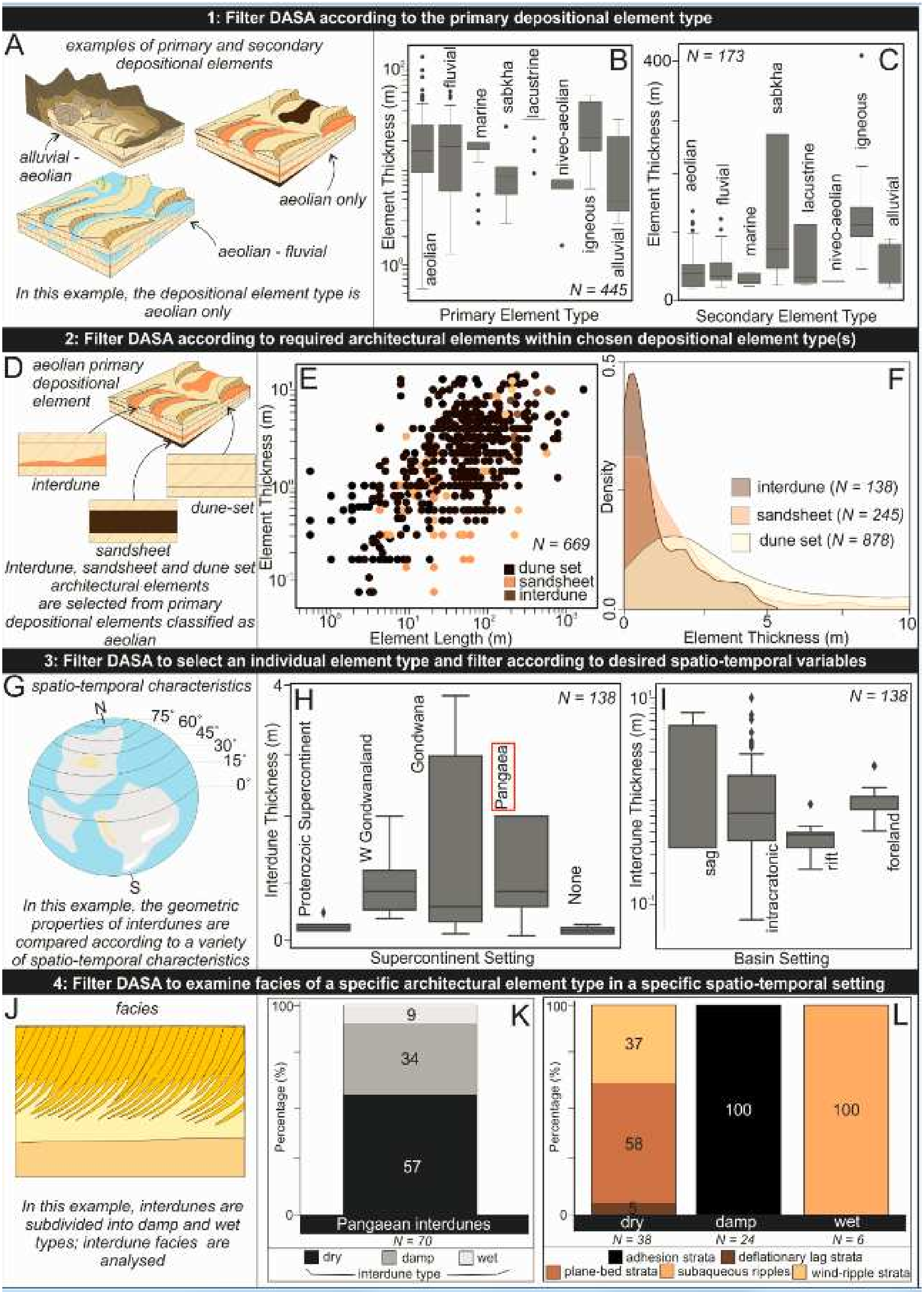
1: Filter DASA according to the primary depositional element type
A
examples of primary and secondary depositional elements
alluvial - aeolian
aeolian only
aeolian - fluvial
In this example, the depositional element type is aeolian only
B
Element Thickness (m)
aeolian
fluvial
marine
sabkha
lacustrine
niveo-aeolian
igneous
alluvial
N = 445
Primary Element Type
C
N = 173
Element Thickness (m)
aeolian
fluvial
marine
sabkha
lacustrine
niveo-aeolian
igneous
alluvial
Secondary Element Type
2: Filter DASA according to required architectural elements within chosen depositional element type(s)
D
aeolian primary depositional element
interdune
dune-set
sandsheet
Interdune, sandsheet and dune set architectural elements are selected from primary depositional elements classified as aeolian
E
Element Thickness (m)
N = 669
dune set
sandsheet
interdune
Element Length (m)
F
Density
interdune (N = 138)
sandsheet (N = 245)
dune set (N = 878)
Element Thickness (m)
3: Filter DASA to select an individual element type and filter according to desired spatio-temporal variables
G
spatio-temporal characteristics
N
S
In this example, the geometric properties of interdunes are compared according to a variety of spatio-temporal characteristics
H
N = 138
Interdune Thickness (m)
Proterozoic Supercontinent
W Gondwanaland
Gondwana
Pangaea
None
Supercontinent Setting
I
N = 138
Interdune Thickness (m)
sag
intracratonic
rift
foreland
Basin Setting
4: Filter DASA to examine facies of a specific architectural element type in a specific spatio-temporal setting
J
facies
In this example, interdunes are subdivided into damp and wet types; interdune facies are analysed
K
Percentage (%)
9
34
57
Pangaean interdunes
N = 70
dry
damp
wet
interdune type
L
Percentage (%)
37
58
5
100
100
dry
damp
wet
N = 38
N = 24
N = 6
adhesion strata
deflationary lag strata
plane-bed strata
subaqueous ripples
wind-ripple strata

Table 1

Case Number	Case Study Name	Location	Reference(s)
1	Grand Erg Oriental	Algeria, Tunisia	McKee (1979); Al-Masrahy and Mountney (2015); Telbisz and Kesler (2018)
2	Atlantic Sahara	Morocco	Elbelrhiti et al. (2008)
3	Idhan Murzuk	Libya	Al-Masrahy and Mountney (2015)
4	El Djouf	Mauritania, W Africa	Al-Masrahy and Mountney (2015)
5	Kalahari Desert	Botswana, Namibia, South Africa	McKee (1979); Kalahari (1988)
6	Namib Desert	Angola, Namibia, South Africa	McKee (1979); Lancaster (2009); White et al. (2011); Al-Masrahy and Mountney (2015); White et al. (2015)
7	An Nafud	Saudi Arabia	McKee (1979);
8	Western Desert	Egypt	Hamdan et al. (2016)
9	Persian Gulf	United Arab Emirates	McKee (1979);
10	Wahiba Sands	Oman	Al-Masrahy and Mountney (2015)
11	Rub’ Al Kali	Saudi Arabia, Oman, United Arab Emirates, Yemen	McKee (1979); Al-Masrahy and Mountney (2013); Al-Masrahy and Mountney (2015);
12	Karakum	Turkmenistan	McKee (1979);
13	Kharan Desert	Pakistan	Al-Masrahy and Mountney (2015)

14	Thar Desert	India, Pakistan	McKee (1979); Bhadra et al. (2019)
15	Taklamakan Desert	Xinjiang, China	McKee (1979); Dong et al. (2000)
16	Gobi Desert	China, Mongolia	McKee (1979); Al-Masrahy and Mountney (2015)
17	Mu Us Desert	China	Al-Masrahy and Mountney (2015)
18	Great Sandy Desert	Australia	Wasson and Hyde (1983)
19	Simpson Desert	Australia	McKee (1979); Nanson and Price (1995); Al-Masrahy and Mountney (2015)
20	Strzelecki Desert	Australia	Wasson and Hyde (1983); Bishop (1997)
21	Victoria Valley	Antarctica	Bourke et al. (2005)
22	Colorado Desert	California, USA	Long and Sharp (1964); Bishop (1997)
23	Algodones Dunes	USA, Mexico	McKee (1979);
24	Sonora Desert (Gran Desierto)	Mexico	McKee (1979);
25	Navajo Indian Reservation	Arizona, USA	McKee (1979);
26	White Sands	New Mexico, USA	McKee (1979); Baitis et al. (2014); Al-Masrahy and Mountney (2015)
27	Atacama Desert	Chile, Peru	Finkel (1959)
28	Monte Desert	Argentina	Al-Masrahy and Mountney (2015)

2034 Table 2

Case Number	Case Study Name	Location	Reference(s)
1	Eriksfjord Formation	Greenland	Clemmensen (1988)
2	Hopeman Sandstone	Scotland, UK	Clemmensen (1987)
3	Arran Red Beds	Isle of Arran, Scotland, UK	Clemmensen and Abrahamsen (1983)
4	Sherwood Sandstone	UK (Onshore and Offshore England and Northern Ireland)	Cowan (1993); Meadows and Beach (1993)
5	Rotliegendes Sandstone	Germany, Poland, Denmark, Baltic Sea, Netherlands	Ellis (1993); Newell (2001)
6	Boxtel Formation	Netherlands, Germany, Denmark, Poland	Schokker and Koster (2004)
7	Sable de Fontainbleau Formation	France	Cojan and Thiry (1992)
8	Escorihuela Formation	NE Spain	Liesa et al. (2016)
9	Etjo Formation	Namibia	Mountney and Howell (2000)
10	Tsondab Sandstone	Namibia	Kocurek et al. (1999)
11	Egalapenta Formation	India	Biswas (2005); Dasgupta et al. (2005)
12	Tumblagooda Formation	Australia	Trewin (1993)
13	Tamala Limestone	Australia	Semeniuk and Glassford (1988)
14	Sao Sebastiao Formation	Brazil	Formolo Ferronatto et al. (2019)
15	Sergi Formation	Brazil	Scherer et al. (2007)
16	Mangabeira Formation	Brazil	Ballico et al. (2017)
17	Caldeirao Formation	Brazil	Jones et al. (2015)

18	Bandeirinha Formation	Brazil	Simplicio and Basilici (2015)
19	Guara Formation	Brazil	Scherer and Lavina (2005)
20	Piramboia Formation	Brazil	Dias and Scherer (2008)
21	Huitrin Formation	Argentina	Stromback et al. (2005)
22	Agrio Formation	Argentina	Veiga et al. (2002)
23	Rio Negro Formation	Argentina	Zavala and Frieje (2001)
24	Copper Habor Formation	Michigan, USA	Taylor and Middleton (1990)
25	Chugwater Formation	Wyoming, USA	Irmen and Vondra (2000)
26	Arikaree Formation	Wyoming, Nebraska, USA	Bart (1977)
27	Ingleside Formation	Colorado, Wyoming, USA	Pike and Sweet (2018)
28	Lower Cutler Beds	Utah, USA	Jordan and Mountney (2010)
29	Cedar Mesa Sandstone	Utah, Colorado, New Mexico, Arizona, USA	Loope (1985); Mountney and Jagger (2004)
30	Navajo Sandstone	Nevada, Arizona, Colorado, Utah, USA	Loope and Rowe (2003)
31	Entrada Sandstone	Wyoming, Utah, Arizona, New Mexico, Texas, USA	Crabaugh and Kocurek (1993); Benan and Kocurek (2000); Kocurek and Day (2018);
32	Big Bear Formation	California, USA	Stewart (2005)
33	Wolfville Formation	Nova Scotia, Canada	Leleu and Hartley (2018)

34	Page Sandstone	Arizona, Utah, Wyoming, USA	Jones and Blakey (1997); Kocurek et al. (1992)

Table 3

Depositional Complexes	**Description**
Aeolian	Deposits arising from, or relating to, the action of wind.
Niveo-Aeolian	Deposits composed of mixed aeolian and snow deposits, typically found in cold-climate settings (Koster and Dijkmans, 1988; McKenna-Neuman, 1990).
Fluvial	Deposits arising from or relating to the action of streams and rivers.
Marine	Deposits arising from or relating to the action of the sea.
Alluvial	Deposits arising from, or relating to the action of streams and sediment gravity-flow processes (cf. Melton, 1965).
Lacustrine	Deposits arising from or relating to accumulation in perennial lakes.
Sabkha/Playa Lake	Sabkhas and playa lakes describe low-relief flats where evaporites, and in some cases carbonates, accumulate. The terms sabkha and playa lake were originally used to describe coastal and inland settings, respectively (Evans, et al., 1964; Purser and Evans, 1973); however, the terms are now used interchangeably.
Igneous	Deposits relating to intrusive or extrusive volcanic activity.
Other	Any depositional element that differs in origin from those above.

Table 4

Architectural or Geomorphic Element Type	**Description**
Dune (A/G)	Dunes are large (wavelengths of 5–250 m; Wilson, 1971, 1972) masses of wind-blown sand, typically found in desert and coastal environments (McKee; 1979). Dunes are classified further according to dune type.
Megabedform or Draa (A/G)	Megabedforms or Draas are very large (wavelengths of 500–5000 m and heights >50 m; Wilson, 1971, 1972) bed forms that are compound or complex in form (*sensu* McKee, 1979) where they support the development of superimposed dune-scale bed forms.
Cross-strata package (A)	Packages of aeolian stratification (typically composed of wind-ripple, grainflow and grainfall strata; Hunter 1977, 1981); form parts of dune sets; packages of cross-strata are typically separated by reactivation surfaces (Brookfield, 1977; Kocurek, 1996).

Dune set (A)	Dune-sets form the fundamental unit of deposition of an aeolian sand dune; dune-sets are formed of packages of cross-strata (Sorby, 1859; Allen, 1963; Rubin and Hunter 1982; Chrintz and Clemmensen, 1993); if dune sets migrate over each other, cross-stratified packages are truncated, delineating sets that are bounded by erosional surfaces (Brookfield, 1977; Kocurek, 1996).
Dune coset (A)	Two or more genetically related dune sets that occur in vertical succession; both the coset and its contained sets are separated by bounding surfaces (Brookfield, 1977; Kocurek, 1996).
Dune compound set (A)	A specialized class of coset wherein the contained sets record the migration of formative bed forms of a *common type*, for example where dunes migrate over the flanks of a parent megabedform (draa) which is itself migrating to leave an accumulation; both the compound set and its contained sets are separated by bounding surfaces (Brookfield, 1977; Kocurek, 1996).
Sandsheet (A/G)	Sandsheet deposits are low-relief accumulations of aeolian sediment in areas where dunes are generally absent (Kocurek and Nielsen, 1986; Brookfield, 1992; Rodríguez-López et al., 2012); can include low-relief bedforms such as zibar.
Interdune (undifferentiated) (A/G)	Interdune deposits are formed in the low-relief, flat, or gently sloping areas between dunes; neighbouring dunes are separated by interdunes; commonly referred to as the interdune corridors, interdune areas, or interdune hollows (Hummel and Kocurek, 1984).
Dry interdune (A/G)	Dry interdunes are characterized by deposits that accumulate on a substrate where the water table is well below the ground surface, such that sedimentation is not controlled by and is largely not influenced by the effects of moisture (Fryberger et al., 1990).
Damp interdune (A/G)	Damp interdunes are characterized by deposits that accumulate on a substrate where the water table is close to the ground surface, such that sedimentation is influenced by the presence of moisture (Fryberger et al., 1988; Lancaster and Teller, 1988; Kocurek et al., 1992).
Wet interdune (A/G)	Wet interdunes are characterized by deposits that accumulate on a substrate where the water table is elevated above the ground surface such that the interdune is episodically or continuously flooded with water (Kocurek and Havholm, 1993; Loope et al., 1995; García-Hidalgo et al., 2002).

Table 5

Facies Element Type	**Description**
Wind-ripple strata	Wind-ripple lamination forms when wind-blown, saltating grains strike sand-grains obliquely and propel other grains forward (Bagnold, 1941; Hunter, 1977). The foreset laminae of wind-ripple strata are occasionally preserved (rippleform laminae), however, the internal laminae of wind-ripple strata are often indistinguishable due to grain size uniformity (translatent wind-ripple stratification; Hunter, 1977). In DASA, wind-ripples are subdivided into

	subcritically, critically and supercritically climbing ripple forms (*sensu* Hunter, 1977).
Grainflow strata	Grainflow strata form where a dune slipface undergoes gravitational collapse (Hunter, 1977; Mountney, 2006b; Bristow and Mountney, 2013). Grainflow deposits are typically erosionally based and are devoid of internal structure. Grainflow strata typically form discrete tongues or wide sheets of inclined strata on the lee-slope of dunes, which wedge-out towards the base of the dune; individual grainflow strata may be indistinguishable, resulting in amalgamated grainflow units (Howell and Mountney, 2001).
Grainfall strata	Grainfall strata are gravity-driven deposits that occur when the wind transports saltating clouds of grains beyond a dune brink; grains settle onto the upper portions of lee slopes as wind transport capacities reduce in the lee-side depressions (Nickling et al., 2002). Grainfall laminae are typically thin (<1 mm), drape existing topography, else may have a wedge-shaped geometry; grainfall lamination is generally composed of sand and silt or (rarely) clay sizes grains (Hunter, 1977).
Interfingered strata	Cross-bedded strata are pervasive in aeolian dune sands and form through recurrent sedimentation on lee-slopes. Alternating processes of deposition give rise to intercalated (interfingering) pacakges of wind-ripple, grainflow and grainfall strata (Hunter, 1977; Hunter, 1981). Planes of stratification record the former shape and location of the lee-slope (Kocurek and Dott, 1981; Fryberger and Schenk, 1981). This composite facies type is used only in cases where it is not possible to differentiate individual wind-ripple, grainflow and grainfall facies elements.
Adhesion strata	Adhesion strata results from the adhesion of moving grains to a damp surface, such as a damp interdune (Hummel and Kocurek, 1984). Adhesion strata typically are low relief (several mm in height) and exhibit sub-horizontal structures with irregular surfaces. In DASA, adhesion strata can be further subdivided into adhesion plane beds, adhesion ripples (Kocurek and Fielder, 1982) and adhesion warts (Olsen et al., 1989), where appropriate.
Plane-bed strata	Plane-bed lamination forms when wind velocities are too high to form ripples (Hunter 1977, 1980). Plane-bed lamination is composed of (sub)horizontally laminated sand, which typically dips at angles of between 0 and 15° (Pye, 2009). Plane-bed laminae are typically millimetre-scale, with sharp or gradational contacts (e.g., Clemmensen and Abrahamsen, 1983) and form sets typically up to 100 mm (Pye, 2009).
Subaqueous ripple strata	Subaqueous ripple lamination is generated by tractional processes and are produced by the action of waves or currents on a sediment surface (Allen, 1978).

Table Captions

Table 1: Modern case-studies included in DASA

Table 2: Ancient case-studies included in DASA

Table 3: Depositional complex types used in DASA for the classification of depositional settings. Each depositional complex type can be used as a primary or secondary complex type descriptor.

Table 4: Examples of DASA sub-environment and architectural-element types for the classification of architectural and geomorphic elements; only the aeolian architectural and geomorphic elements discussed in this article are included here. A full account of all types of architectural and geomorphic elements included in DASA is available in the Supplementary Information.

Table 5: Examples of DASA facies types for the classification of facies elements; only the facies elements discussed in this article are included here. A full account of all DASA facies types is available in the Supplementary Information.